Damage-associated molecular pattern scoring system and its role in prognosis and immunotherapy in hepatocellular carcinoma

HU Hao[1], YUAN Lehong[2], SONG Zewen[1], TAN Juan[3], NI Zixuan[3], LIU Yang[3], ZHANG Xi[1]

(1. Department of Oncology, Third Xiangya Hospital, Central South University, Changsha 410013;
2. Department of Emergency, Third Xiangya Hospital, Central South University, Changsha 410013;
3. Department of Pathology, Third Xiangya Hospital, Central South University, Changsha 410013, China)

ABSTRACT

Objective: Significant interindividual differences exist in the efficacy of immunotherapy for hepatocellular carcinoma (HCC), and reliable biomarkers for predicting therapeutic response are lacking. Immunogenic cell death (ICD) participates in regulating the tumor immune microenvironment (TME) through the release of damage-associated molecular patterns (DAMPs), thereby possessing the potential to reshape the TME. DAMPs are essential for the occurrence of ICD. This study aims to address the lack of systematic evaluation of ICD-related molecular subtypes in HCC by constructing a DAMP-related molecular classification system and risk scoring model, as well as identifying hub genes regulating ICD in HCC for prognosis assessment and prediction of immunotherapy response.

Methods: Transcriptomic data and clinical information from multiple cohorts, including The Cancer Genome Atlas (TCGA)-LIHC dataset, the Gene Expression Omnibus (GEO) GSE14520 dataset, and the International Cancer Genome Consortium (ICGC)-LIRI dataset, were integrated. Unsupervised consensus clustering analysis of 40 DAMP-related genes was performed to identify molecular subtypes of HCC, followed by functional analyses and identification of activated signaling pathways in each subtype. Prognosis-related genes were screened from differentially expressed genes using univariate Cox regression analysis, and a DAMP scoring model was established through least absolute shrinkage and selection operator (LASSO) regression and stepwise Cox regression analyses. The ESTIMATE algorithm was used to evaluate TME characteristics, and the CIBERSORT algorithm was applied to analyze immune cell infiltration levels in HCC. Time-dependent receiver operating characteristic (ROC) curve analysis was used to evaluate the prognostic predictive performance of the DAMP score and compare it with clinical characteristics and

Date of reception: 2025-10-27

First author: HU Hao, Email: huhao91@csu. edu. cn, ORCID: 0009-0005-2468-5483; YUAN Lehong, Email: yuanlehong9765@csu. edu. cn, ORCID: 0009-0006-1457-6168

Corresponding author: LIU Yang, associate professor, Email: 601032@csu. edu. cn, ORCID: 0000-0002-0367-8189; ZHANG Xi, associate professor, Email: xy3zhangxi@csu.edu.cn, ORCID: 0000-0002-1712-8217

Foundation item: This work was supported by the Natural Science Foundation of Hunan Province, China (2022JJ30896).

Open access: This is an open access article under Creative Commons Attribution-NonCommercial-NoDerivatives 4.0 International (CC BY-NC-ND 4.0) (https://creativecommons.org/licenses/by-nc-nd/4.0/).

©Journal of Central South University (Medical Science). All rights reserved.

previously published messenger RNA (mRNA) biomarkers. Weighted gene co-expression network analysis (WGCNA) was used to identify hub genes associated with the DAMP score. Immunohistochemistry (IHC) staining was performed to validate differential expression of hub genes between tumor and normal tissues. In vitro experiments, including cell counting kit-8 (CCK-8) assays and wound-healing assays, were conducted to investigate the role of hub genes in HCC. Flow cytometry was used to detect apoptosis levels and evaluate sensitivity to the ICD inducer 5-fluorouracil (5-FU).

Results: Unsupervised consensus clustering analysis showed that HCC patients could be classified into 2 subgroups, namely low-DAMP-score and high-DAMP-score groups, based on the expression profiles of DAMP-related genes. Patients in the low-DAMP-score group had longer overall survival and exhibited higher immune cell infiltration, particularly $CD8^+$ T-cell infiltration (all $P<0.05$). The DAMP score demonstrated stable prognostic stratification capability across multiple independent cohorts, with poorer survival outcomes observed in the high-DAMP-score group (all $P<0.05$). Time-dependent ROC analysis demonstrated high accuracy of the DAMP score in predicting 1-year and 3-year survival, outperforming commonly used clinical characteristics and 53 previously published mRNA biomarkers. Functional analyses revealed that pathways activated in the high-DAMP-score group were mainly enriched in cell proliferation-related pathways, whereas the low-DAMP-score group was associated with immune activation and metabolism-related pathways. In addition, the DAMP score was significantly negatively correlated with immune cell infiltration levels, and the proportions of multiple immune cell types differed significantly between the high- and low-DAMP-score groups (all $P<0.05$). The DAMP-score-related hub gene *TRIP13* was significantly upregulated in HCC tissues and promoted proliferation and migration of HCC cells (all $P<0.05$). Silencing *TRIP13* expression in HCC cells increased sensitivity to the ICD inducer 5-FU and was accompanied by increased apoptosis levels (all $P<0.05$).

Conclusion: The prognostic risk scoring model constructed based on DAMP-related genes can effectively stratify HCC patients and is closely associated with characteristics of the tumor immune microenvironment. The DAMP scoring model established in this study may be used for prognostic evaluation and prediction of immunotherapy efficacy in HCC and demonstrated stable predictive performance across multiple cohorts. As a hub gene in this DAMP scoring model, *TRIP13* exerts oncogenic effects in HCC and regulates tumor cell sensitivity to the ICD inducer 5-FU. The DAMP-score-based subtype classification system and *TRIP13*-targeted therapy provide new molecular evidence for individualized treatment of HCC.

KEY WORDS immunogenic cell death; damage-associated molecular patterns; *TRIP13*, hepatocellular carcinoma; immunotherapy

损伤相关分子模式评分系统在肝细胞癌预后和免疫治疗预测中的作用

胡昊[1]，袁乐宏[2]，宋泽文[1]，谭娟[3]，倪子旋[3]，刘杨[3]，张曦[1]

©Journal of Central South University (Medical Science). All rights reserved.

(1. 中南大学湘雅三医院肿瘤科，长沙 410013；2. 中南大学湘雅三医院急诊科，长沙 410013；
3. 中南大学湘雅三医院病理科，长沙 410013)

[摘 要] 目的：肝细胞癌(hepatocellular carcinoma，HCC)的免疫治疗效果存在显著的个体差异，缺乏可靠的生物标志物用于疗效预测。免疫原性细胞死亡(immunogenic cell death，ICD)通过激活损伤相关分子模式(damage-associated molecular pattern，DAMP)参与调控肿瘤免疫微环境，其具有改变免疫抑制性肿瘤微环境(tumor microenvironment，TME)的潜力。DAMP对ICD的发生至关重要。本研究旨在针对HCC中ICD相关的分子分型缺乏系统评估的问题，构建基于DAMP相关基因的分型系统及风险评分模型，并识别在HCC中调控ICD的枢纽基因，以用于预后评估及免疫治疗反应预测。**方法：**整合癌症基因组图谱(The Cancer Genome Atlas，TCGA)-LIHC数据集、基因表达综合数据库(Gene Expression Omnibus，GEO)的GSE14520数据集及国际癌症基因组联盟(International Cancer Genome Consortium，ICGC)-LIRI数据集等多队列的转录组数据及临床信息，对40个DAMP相关基因进行无监督共识聚类分析，识别HCC分子亚型，进行功能分析，并识别各个亚型中被激活的信号通路。采用单因素Cox回归分析法从差异表达基因中筛选预后相关基因，并通过最小绝对收缩与选择算子(least absolute shrinkage and selection operator，LASSO)回归及逐步Cox回归分析法建立DAMP评分模型。采用ESTIMATE算法评估TME特征，CIBERSORT算法分析HCC的免疫细胞浸润水平。采用时间依赖性的受试者操作特征曲线(receiver operator characteristic curve，ROC)分析DAMP评分的预后预测能力，并与临床特征及既往发表的信使RNA(messenger RNA，mRNA)标志物进行比较。利用加权基因共表达网络分析(weighted gene co-expression network analysis，WGCNA)筛选与DAMP评分相关的枢纽基因。通过免疫组织化学(immunohistochemistry，IHC)染色验证枢纽基因在肿瘤组织和正常组织中的表达差异，并结合体外实验[包括细胞计数试剂盒-8(cell counting kit-8，CCK-8)和细胞划痕试验]探讨枢纽基因在HCC中的作用，同时采用流式细胞术检测细胞凋亡水平，以评估枢纽基因对ICD诱导剂5-氟尿嘧啶(5-fluorouracil，5-FU)的敏感性。**结果：**无监督共识聚类分析结果表明，基于DAMP相关基因的表达特征，HCC患者可分为低DAMP评分和高DAMP评分2个亚组。其中低DAMP评分组的总生存期更长，且具有高免疫细胞浸润特征(尤其是$CD8^+$ T细胞)(均P<0.05)。DAMP评分在多个独立队列中均表现出稳定的预后分层能力，高DAMP评分组的生存结局较差(均P<0.05)。时间依赖性ROC分析显示，DAMP评分在1年和3年生存预测中具有较高准确性，其预测效能优于常用的临床特征及53个已发表的mRNA标志物。功能分析表明，高DAMP评分组中被激活的通路主要富集于细胞增殖相关通路，而低DAMP评分组则与免疫激活及代谢有关通路相关。同时，DAMP评分与免疫细胞浸润水平呈显著负相关，高DAMP评分组与低DAMP评分组相比，多种免疫细胞的比例均显著改变(均P<0.05)。DAMP评分相关的枢纽基因*TRIP13*在HCC组织中显著上调，并可促进HCC细胞的增殖和迁移(均P<0.05)。沉默HCC细胞中*TRIP13*的表达可增加对ICD诱导剂5-FU的敏感性，并伴随细胞凋亡水平的升高(均P<0.05)。**结论：**基于DAMP相关基因构建的预后风险评分模型能够对HCC患者进行有效分层，并与肿瘤免疫微环境特征密切相关。本研究建立的DAMP评分模型可用于HCC的预后评估及免疫治疗的效果预测，并在多队列中显示出稳定的预测性能。*TRIP13*作为该模型中的枢纽基因，在HCC中发挥促癌作用，并调控肿瘤细胞对ICD诱导剂5-FU的敏感性。基于DAMP评分的亚型分型系统和*TRIP13*靶向治疗为HCC的个体化治疗提供了新的分子依据。

[关键词] 免疫原性细胞死亡；损伤相关分子模式；*TRIP13*；肝细胞癌；免疫疗法

Hepatocellular carcinoma (HCC), one of the most common cancers in the world, is the major primary malignancy of the liver. It has a high incidence rate and fatality rate in both men and women[1], and the incidence rate is currently on the rise. The pathogenesis of hepatocellular carcinoma is complex, but it usually develops in the order of liver injury, chronic inflammation, lipid degeneration, fibrosis, cirrhosis and HCC step by step[2]. The traditional treatment of HCC includes surgical resection, liver transplantation, and transcatheter arterial chemoembolization, but these therapies have poor efficacy for patients with advanced cancer and are partly dependent on whether effective donors can be used. Due to cirrhosis, many cytotoxic drugs cannot be applied, and HCC is resistant to many drugs, which makes it difficult to develop a promising chemotherapy regimen for liver cancer[3].

At present, immunotherapy has shown a noticeable effect in the treatment of some malignant tumors. The body has the innate immune system and the adaptive immune system, which can effectively recognize and kill tumor cells. When the immune cells of the body

©Journal of Central South University (Medical Science). All rights reserved.

cannot recognize the tumor cells or the immune function is inhibited, immune escape occurs and it will facilitate the development of cancer. Like other tumors, HCC also escapes anti-tumor immune response by expressing corresponding ligands. This provides a new way for the treatment of advanced HCC[4]. Currently, the main immunotherapies for HCC include adoptive cell therapy, HCC cell vaccines, immune checkpoint inhibitors (ICIs) and oncolytic virotherapy. Although these immunotherapies have produced certain effects on HCC, there are also many difficulties and problems[5-7].

Immunogenic cell death (ICD) is a kind of cancer cell death caused by some chemotherapy drugs, oncolytic viruses, photodynamic therapy and radiotherapy[8]. The main feature is that tumor cells change from non-immunogenicity to immunogenicity and induce anti-tumor immune response. ICD is characterized by the release of damage-associated molecular pattern (DAMP), including calreticulin (exposed on the cell surface), adenosine triphosphate (ATP), heat-shock proteins (HSP) 70, HSP90, high mobility group box-1 (HMGB1) and others. These DAMPs will release during ICD activates the tumor-specific immune response, thus killing tumor cells to achieve an anti-cancer effect[9].

Currently, several ICD-based anti-cancer drugs have been approved for the treatment of adult patients with recurrent or refractory malignancies, like multiple myeloma and small cell lung cancer, via potential mechanisms that enhance the anti-tumor response mediated by T cells[10-12]. However, not all patients might respond well to these ICD inducers. For instance, tumor cells in mice presenting with genetic defects in Toll-like receptor (TLR) 4 or myeloid differentiation primary response protein 88 (MyD88) did not show immunogenicity after exposure to ICD-inducers[13]. Notably, studies[14-17] have shown that prognostic models based on ICD or DAMP-related signatures could demonstrate excellent ability in predicting overall survival (OS) and guiding anti-tumor therapies in cancers. For example, the molecular clusters related to ICD and the risk model of ICD can effectively predict the prognosis and immunotherapy response of glioma, providing great help for future treatment strategies of this disease[16], and the ICD-score signatures also perform well in evaluating the prognosis and predicting treatment response of gastric cancer patients[18]. Therefore, screening biomarkers and establishing new features based on ICD or DAMP-related genes may provide new useful choices for the treatment and prognosis of HCC in the future.

Since DAMP is the core for the occurrence of ICD, we aim to explore the role of DAMP-related genes in HCC by integrating bioinformatics analyses with *in vitro* experiments. We constructed a novel DAMP-related risk score (DAMP score) and compared it with previously established messenger RNA (mRNA) signatures. Furthermore, we investigated the correlation between the DAMP score and immune cell infiltration (particularly $CD8^+$ T cells), with the goal of developing a more effective tool for predicting immunotherapy sensitivity.

1 Materials and methods

1.1 Ethics statements

The study protocol was approved by the Ethics Committee of the Third Xiangya Hospital of Central South University (Approval number: 2023-S005). Written informed consent was obtained from these patients before tissues collection.

1.2 Public data acquisition and processing

Gene expression data, phenotype data, and survival information of The Cancer Genome Atlas (TCGA) - LIHC, Gene Expression Omnibus (GEO) GSE14520, and International Cancer Genome Consortium (ICGC) - LIRI cohorts were downloaded. The gene expression data of GSE35640 and GSE64041 were also downloaded from the GEO database. The transcriptional data and clinical information of the Riaz17 study, Liu19 study, VanAllen15 study, Peking University Cancer Hospital (PUCH) study and Gide19 study were downloaded from the GitHub[19]. All of the data were processed as reported in our previous studies[20-21]. To explore whether DAMP-related genes help to stratify subgroups of HCC patients, consensus clustering was first conducted based on the transcriptional expression of 40 DAMP-related genes (supplementary Table 1, https://doi.org/10.57760/sciencedb.32748), which were collected from 2 previously published studies[17, 22].

©Journal of Central South University (Medical Science). All rights reserved.

1.3 Consensus clustering

Consensus clustering was conducted by using the "ConsensusClusterPlus" package in R[23]. The parameters used in the analyses were K_{max}=10, reps=1 000, pItem=0.8, pFeature=1, clusterAlg= "pam", corUse="complete.obs", and seed=123456.

1.4 Construction of the DAMP score in HCC

The differentially expressed genes (DEGs) between the 2 subgroups identified by consensus clustering were analysed using the "limma" package in R. These DEGs then underwent univariate Cox regression analyses, and those genes with a prognostic P<0.1 in the TCGA-LIHC and GSE14520 cohorts were input into a least absolute shrinkage and selection operator (LASSO) regression model in TCGA-LIHC cohort. The screened genes were further input into a stepwise Cox regression model (bidirectional elimination). The generated crucial genes and their corresponding coefficient were used to calculate the risk score for each patient based on the following formula: risk score $=\sum_i \text{coefficient}(\text{Gene}\,i)*\text{expression}(\text{Gene}\,i)$. The DAMP score of patients in each cohort was then calculated by the formula: DAMP score $=(\text{score}-\text{Min})/\text{absolute}(\text{Max})$, as reported in our previous studies[21, 24]. We compared the C-index of DAMP score and that of 53 previously published mRNA signatures (supplementary Table 2, https://doi.org/10.57760/sciencedb. 32748) retrieved from the PubMed. These signatures were constructed based on multiple biological processes, including hypoxia[25-26], N^6-methyladenosine (m^6A) RNA methylation[27], pyroptosis[28], ferroptosis[29], among others. To further characterize the biological differences between HCC patients stratified by the DAMP score, we compared pathway activation and the tumor micro-environment (TME) between the high- and low-DAMP score groups (defined by the median score) (supplementary Table 3, https://doi.org/10.57760/sciencedb.32748). Since no data about HCC patients receiving immunotherapy was currently available for analyses in this work, we tested the predictability of DAMP score in melanoma patients receiving immunotherapy. Further, Genomics of Drug Sensitivity in Cancer (GDSC) database was used to predict potential targeted therapy for DAMP score-stratified HCC subgroups.

1.5 Immune profile analysis

The immune, stromal and ESTIMATE scores of HCC patients were calculated by the "estimate" package in R, based on the transcriptional expression of selected immune-related genes[30]. The tumor purity was calculated by the formula reported in the study[30]: Tumor purity =cos(0.604 987 201 8+0.000 146 788 4* ESTIMATE score). In addition, the infiltrating level of 22 immune cells, such as $CD8^+$ T cells, M0 macrophages, and neutrophils, in HCC patients was estimated by the CIBERSORT algorithm in R software, as reported in our previous study[21].

1.6 Enrichment analysis

Gene set enrichment analysis (GSEA) of HCC patients was conducted by using the "clusterProfiler" package in R. The visualization of GSEA results was achieved by the "GseaVis" package in R[31]. The "*c5.go.bp.v2022.1.Hs.symbols.gmt*" was selected as the gene set database.

1.7 Cell culture and lentiviral infection

HepG2 and LM3 cells were obtained from the Cell Bank of Shanghai Institute for Biological Sciences, Chinese Academy of Sciences. Cells were cultured in Dulbecco's modified eagle medium (DMEM) containing 10% fetal bovine serum (FBS), and maintained in an incubator with constant temperature and CO_2. Lentivirus was used to infect HepG2 and LM3 cells to produce stable overexpression or knockdown of *TRIP13*. Lentivirus was acquired from Genechem company (Shanghai, China).

1.8 Western blotting

Cells were lysed on ice with pre-cooled radioimmunoprecipitation assay buffer (RIPA) for 10 min, and centrifuged at 4 ℃ for 10 min (12 000 rpm) to obtain the supernatant for subsequent detection. Western blotting was performed using antibodies against glyceraldehyde-3-phosphate dehydrogenase (GAPDH) (#5174, Affinity Biosciences, Beijing, China), B-cell Lymphoma 2 (Bcl-2) (AF6139, Affinity Biosciences, Beijing, China), Bcl-2-associated X protein (Bax) (#41162, Cell Signaling Technology, United States), thyroid hormone receptor interactor 13 (TRIP13) (AF0570, Affinity Biosciences, Beijing, China),

©Journal of Central South University (Medical Science). All rights reserved.

calreticulin (CRT) (DF3139, Affinity Biosciences, Beijing, China), and HMGB1 (AF7020, Affinity Biosciences, Beijing, China). Horseradish peroxidase-labeled Goat anti-rabbit IgG (H+L) (S0001, Affinity Biosciences, Beijing, China) was used as secondary antibody.

1.9 Immunofluorescence staining

Cells were seeded onto the special dish at a density of approximately 30%, then fixed with cold methanol, permeabilized with triton 0.3% X-100, blocked with bovine serum albumin (BSA), incubated with primary and secondary antibodies, stained with 4', 6-diamidino-2-phenylindole (DAPI), and detected by confocal laser scanning microscopy. Goat Anti-Rabbit IgG (H+L) CY3-conjugated (S0011, Affinity Biosciences, Beijing, China) was used as secondary antibody.

1.10 Cell counting kit-8 assay

Cells were placed in 96-well plates. Cell culture medium and cell counting kit-8 (CCK-8) reagent (C0038, Beyotime, China) were prepared as a working solution at a volume ratio of 10: 1. After the residual medium was removed and 100 μL working solution was added, the cells were then incubated at 37 ℃ and detected with microplate reader. Since 5-fluorouracil (5-FU) could induce ICD in HCC[32], it was used to explore the impact of TRIP13 on the sensitivity of HCC cells to ICD.

1.11 Colony formation assay

Cells were seeded onto 6-well plates (500 cells/well) and cultured for 12 d. Cells were fixed by using paraformaldehyde and stained using crystal violet.

1.12 Cell scratch test

Cells were plated in 6-well plates, scratched with a 200 μL pipette tip. After that, the cells were cultured in the medium containing 1% FBS, and photos were taken using an inverted microscope.

1.13 Immunohistochemistry staining

Immunohistochemistry (IHC) staining was performed on the tissue microarray chip according to the procedure reported in our previous study[33]. The primary antibody against TRIP13 for staining was purchased from Abcam, United Kingdom. Two independent pathologists assessed the expression of TRIP13 in all HCC and tumor-adjacent normal samples with the criteria reported in previous studies[33].

1.14 Apoptosis analysis by flow cytometry

Cell apoptosis was detected using an Annexin V-fluorescein isothiocyanate (FITC)/propidium iodide (PI) apoptosis detection kit (KGA1102-10, KeyGEN BioTECH, China) according to the manufacturer's instructions. Briefly, HepG2 and LM3 cells transfected with short hairpin RNA (shRNA) shTRIP13 or shControl were treated with 5-FU or vehicle for 48 h. Subsequently, the cells were harvested, washed twice with cold phosphate buffered saline (PBS), and resuspended in 1× binding buffer. The cell suspension was then incubated with 5 μL of Annexin V-FITC and 5 μL of PI for 10 min at room temperature in the dark. The stained cells were analyzed immediately using a flow cytometer (Agilent NovoCyte3). The fluorescence of Annexin V-FITC was detected in the FITC channel (~530 nm), and PI was detected in its respective red fluorescence channel (~617 nm) upon 488 nm laser excitation. Viable (Annexin V^-/PI^-), early apoptotic (Annexin V^+/PI^-), late apoptotic (Annexin V^+/PI^+), and necrotic (Annexin V^-/PI^+) cell populations were quantified.

1.15 5-Ethynyl-2'-deoxyuridine assay

Cell proliferation was assessed using the BeyoClick™ 5-Ethynyl-2'-deoxyuridine (EdU)-555 Kit (C0075S, Beyotime, China). Cells seeded in confocal dishes were treated as indicated, and then incubated with 10 μmol/L EdU for 2 h. After fixation with 4% paraformaldehyde (15 min, room temperature) and permeabilization, nuclei were counterstained with DAPI (1 μg/mL, 1 min). Samples were mounted with anti-fade medium and imaged by laser confocal microscopy.

1.16 Statistical analysis

Data are expressed as mean±standard deviation. The following packages in R (version 4.1.3) were used for data analyses and visualization, and they were "tidyverse" "ggplot2" "survival" "survivalROC" "survminer" "timeROC" "rms" "msigdbr" "dplyr" "ggalluvial" "VennDiagram" "ggh4x" "ggrepel" "patchwork" "Oncopredict" "CompareC" "enrichplot" "org. Hs. eg. db" "glmnet" "scales" "aplot" "corrplot"

©Journal of Central South University (Medical Science). All rights reserved.

and “pec”. Pearson method was used for correlation analyses. Kaplan-Meier method was used for prognostic analyses. P<0.05 was considered to be statistically significant.

2 Results

2.1 Unsupervised clustering of DAMP-related genes in HCC

According to the consensus cumulative distribution function (CDF) plot (Figure 1A), k=2 was determined to be the optimal value for consensus clustering (Figure 1B). A total of 199 HCC patients were classified into the C1 cluster, and these patients exhibited significantly shorter OS, compared with C2 cluster (P=0.023, Figure 1C). As shown in Figure 1D, the expression analysis of all 40 DAMP-related genes revealed a distinct pattern: 26 genes were significantly downregulated in the C1 cluster compared to the C2 cluster, while 5 genes showed significantly higher expression in C1. The remaining 9 genes exhibited no statistically significant difference between the 2 clusters.

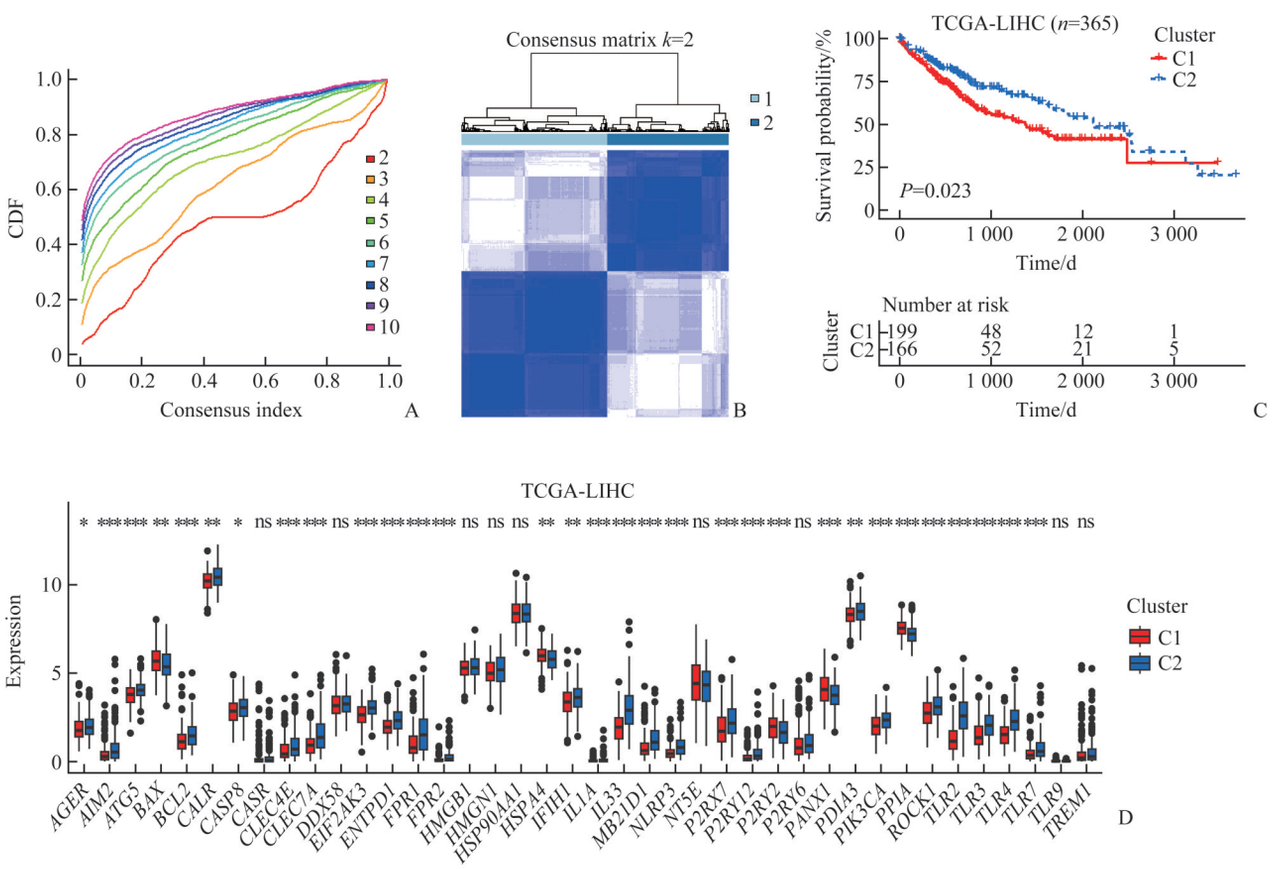


Figure 1 Consensus clustering of HCC patients from TCGA-LIHC cohort based on DAMP-related genes

A: CDF curve of consensus clustering for k=2 to 10; B: Heatmap depicts consensus clustering solution (k=2) for DAMP-related genes in HCC patients; C: Kaplan-Meier curves of OS in the C1 and C2 HCC subgroups; D: Transcriptional expression of DAMP-related genes in the C1 and C2 HCC subgroups. ns: Not significant; *P<0.05, **P<0.01, ***P<0.001. DAMP: Damage-associated molecular pattern; TCGA: The Cancer Genome Atlas; HCC: Hepatocellular carcinoma; CDF: Cumulative distribution function; OS: Overall survival.

2.2 Construction and validation of the DAMP score in HCC

To construct a more applicable DAMP-related signature in HCC, the DEGs between HCC patients in C1 and C2 subgroups were first analyzed (Figure 2A). A total of 225 up-regulated genes and 948 down-regulated

©Journal of Central South University (Medical Science). All rights reserved.

genes met the criteria of absolute fold change ⩾1.5 and adjusted P<0.05 (supplementary Table 4, https://doi.org/10.57760/sciencedb.32748). These DEGs further underwent univariate Cox analyses in the TCGA-LIHC and GSE14520 datasets, and 92 of them had a significant prognostic P<0.1 in both datasets (Figure 2B).

To screen the hub genes representing the difference between C1 and C2 clusters, LASSO Cox regression analyses and subsequently stepwise regression analyses (Figure 2C and 2D) were conducted. Namely, based on the optimal value of λ in the LASSO Cox regression analyses, 19 genes were selected and underwent stepwise regression analyses, which generated 9 hub genes and their corresponding coefficients. The 9 genes were solute carrier organic anion transporter family member 4C1 (*SLCO4C1*), *CD79a* molecule (*CD79A*), peroxisome proliferator-activated receptor gamma coactivator 1 alpha (*PPARGC1A*), granzyme A (*GZMA*), DAB adaptor protein 2 (*DAB2*), vanin 2 (*VNN2*), growth hormone receptor (*GHR*), fascin actin-bundling protein 1 (*FSCN1*), and lecithin-cholesterol acyltransferase (*LCAT*). Based on the transcriptional expression levels and corresponding coefficients of these nine genes, a prognostic score was calculated for each sample using the following formula:

Score= (− 0.15358×*LCAT*) + (0.19842×*FSCN1*) + (−0.13497×*GHR*)+(0.09740×*VNN2*)+(0.19498×*DAB2*)+ (− 0.28657×*GZMA*) + (− 0.18512×*PPARGC1A*) + (−0.14871×*CD79A*)+(0.15484×*SLCO4C1*).

This derived value was designated as the DAMP score for each sample, as detailed in the Methods section. In the training cohort (TCGA-LIHC dataset), HCC patients with high DAMP score (divided by the median value of the DAMP score in the cohort) exhibited significantly shorter median OS than those with low DAMP score (P<0.001, Figure 2E). In 2 validating cohorts, GSE14520 and ICGC-LIRI datasets, HCC patients with high DAMP score (divided by the median value of the DAMP score in each cohort) also had significantly shorter median OS (Figure 2F and 2G).

The time-dependent receiver operating characteristic (ROC) curve analysis results (Figure 3A and supplementary Figure 1A, https://doi.org/10.57760/sciencedb.32748) show that the 1-year and 3-year area under curve (AUC) of the DAMP score were 0.78 and 0.78 in the TCGA-LIHC cohort, 0.72 and 0.74 in the GSE14520 cohort, and 0.77 and 0.69 in the ICGC-LIRI cohort. In both TCGA-LIHC and GSE14520 datasets, the C-index of DAMP score was higher than that of other clinical characteristics, such as tumor stage, Barcelona Clinic Liver Cancer (BCLC) staging, Cancer of the Liver Italian Program (CLIP) staging, AFP, and age (Figure 3B).

As shown in Figure 3C and 3D, the C-index of DAMP score ranked the second and third among those of all the 54 mRNA signatures in the TCGA-LIHC and GSE14520 cohorts, respectively, suggesting DAMP score had superior prognostic predictability compared to most previously published mRNA signatures in HCC.

2.3 Characterization of DAMP score-stratified HCC patients

As shown in Figure 4A to 4I, patients in the high-DAMP score group were predominantly enriched in pathways related to enhanced cell proliferation, including DNA replication (Figure 4A), mitotic sister chromatid segregation (Figure 4B), and mRNA transport (Figure 4C). Conversely, patients in the low-DAMP score group exhibited a distinct functional profile, characterized by enrichment in metabolic processes such as xenobiotic metabolic process (Figure 4D), fatty acid catabolic process (Figure 4E), and cellular amino acid catabolic process (Figure 4F), as well as in multiple immune-active pathways, including phagocytic recognition (Figure 4G), humoral immune response mediated by circulating immunoglobulin (Figure 4H), and B cell receptor signaling pathway (Figure 4I).

The correlation between DAMP score and TME was further evaluated. Indeed, DAMP score showed a significantly negative correlation with stromal score (R= − 0.19, P=0.000 24, Figure 4J) and immune score (R= − 0.23, P=1.4e-05, Figure 4K). Correspondingly, DAMP score exhibited a significantly positive correlation with tumor purity (R=0.22, P=1.7e-05, Figure 4L), suggesting HCC patients with high DAMP score had a low infiltrating level of stromal cells and immune cells. Specifically, CIBERSORT analyses

©Journal of Central South University (Medical Science). All rights reserved.

indicated that patients with high DAMP score had more infiltration of M0 macrophages, whereas patients in the low-DAMP score subgroups had a significantly elevated level of $CD8^+$ T cells, M1 macrophages, and naive B cells (all P<0.05, Figure 4M).

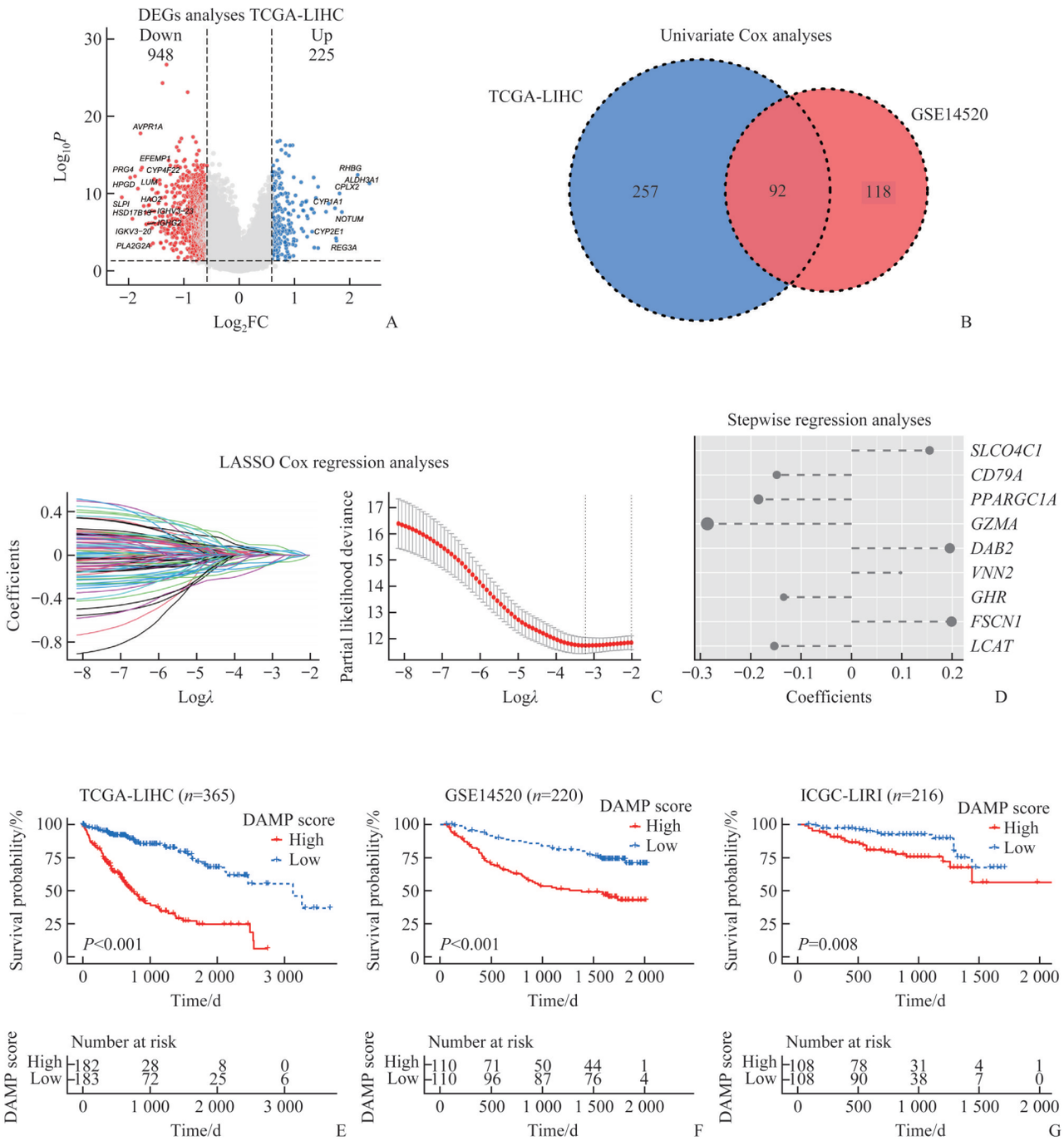


Figure 2 Construction and validation of the DAMP score in HCC

A: Volcano plot of DEGs between the C1 and C2 HCC subgroups from the TCGA-LIHC cohort; B: Venn diagram of DEGs with significant prognostic P<0.1 in the TCGA-LIHC and GSE14520 cohorts; C: LASSO Cox regression model was constructed from 92 common DEGs; D: Stepwise regression analyses identified 9 genes and corresponding coefficients for the construction of the DAMP score; E to G: Kaplan-Meier curves of OS in HCC patients with high- and low-DAMP score from TCGA-LIHC (E), GSE14520 (F), and ICGC-LIRI (G) cohorts. DEGs: Differentially expressed genes; FC: Fold change; LASSO: Least absolute shrinkage and selection operator; ICGC: International Cancer Genome Consortium.

©Journal of Central South University (Medical Science). All rights reserved.

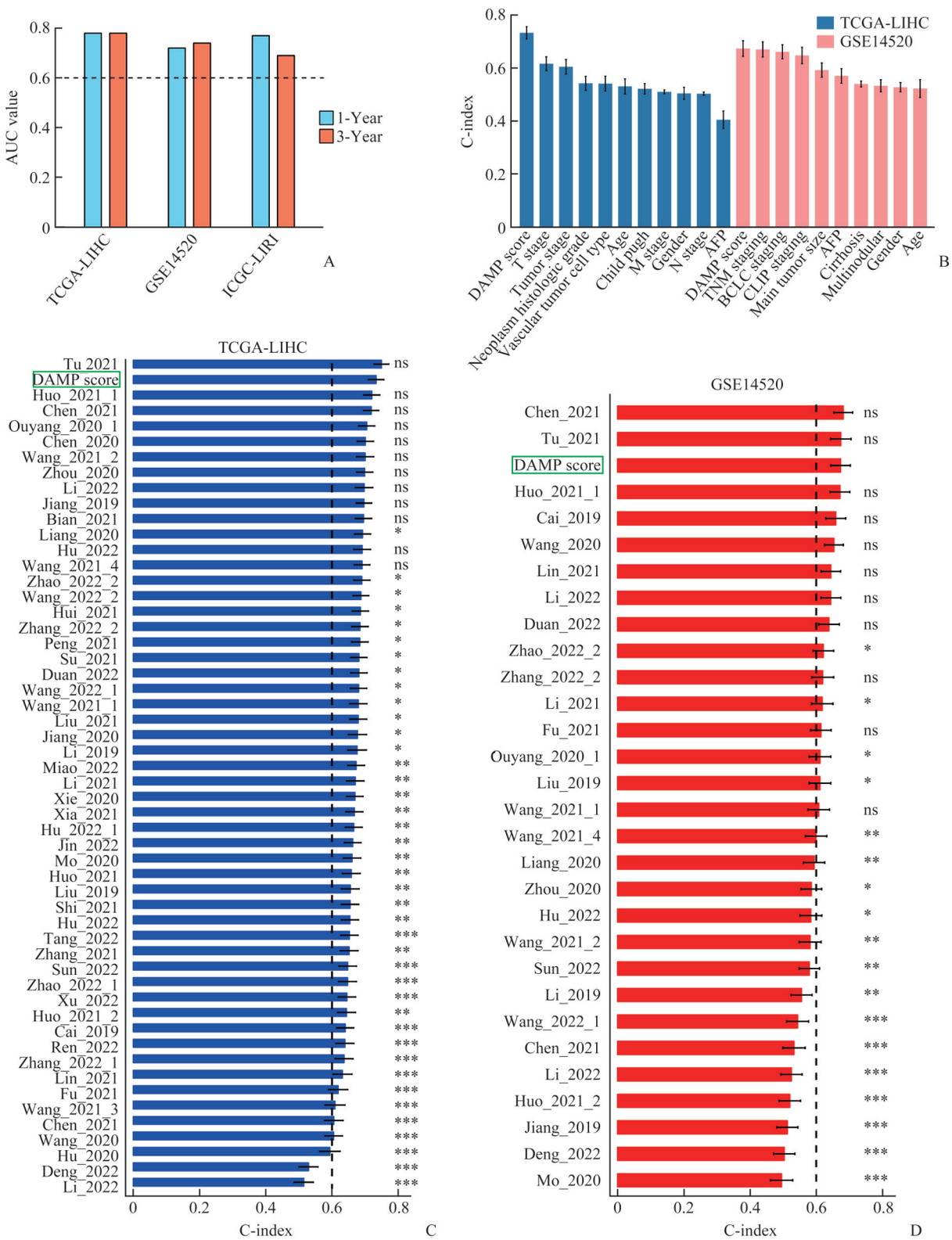


Figure 3 Comparison of DAMP score and other factors in prognostic prediction

A: One-year and 3-year AUC of DAMP score in the TCGA-LIHC, GSE14520, and ICGC-LIRI cohorts. B: C-index (95% confidence interval) of DAMP score and clinical features in the TCGA-LIHC and GSE14520 cohorts. C: C-index (95% confidence interval) of DAMP score and 53 previously published mRNA signatures in the TCGA-LIHC cohort. D: C-index (95% confidence interval) of DAMP score and 52 previously published mRNA signatures in the GSE14520 cohort. ns: Not significant; **P*<0.05, ***P*<0.01, ****P*<0.001. AUC: Area under curve; AFP: Alpha-fetoprotein ; BCLC: Barcelona Clinic Liver Cancer; CLIP: Cancer of the Liver Italian Program.

©Journal of Central South University (Medical Science). All rights reserved.

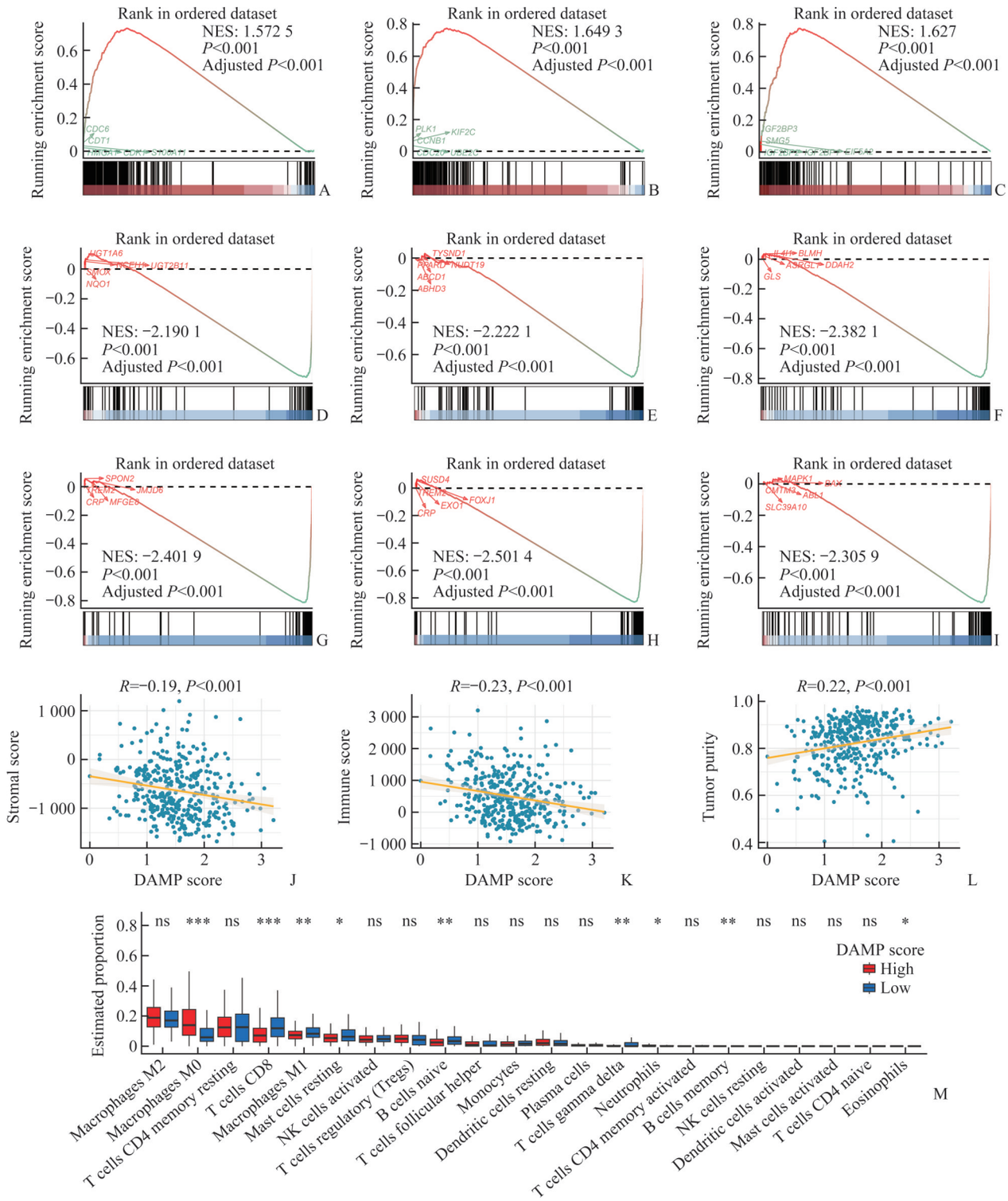


Figure 4 Characterization of DAMP score-stratified HCC patients

A to C: Examples of GSEA results of HCC patients with high-DAMP score, including DNA replication (A), mitotic sister chromatid segregation (B), and mRNA transport (C); D to I: Examples of GSEA results of HCC patients with low-DAMP score, including xenobiotic metabolic process (D), fatty acid catabolic process (E), cellular amino acid catabolic process (F), phagocytic recognition (G), humoral immune response mediated by circulating immunoglobulin (H), and B cell receptor signaling pathway (I). J to L: Correlation between DAMP score and stromal score (J), immune score (K), and tumor purity (L). M: Infiltrating level of 22 types of immune cells in HCC patients with high- and low-DAMP score. The terms for immune cell subsets on the horizontal axis in the figure all use the fixed naming conventions of the CIBERSORT algorithm. ns: Not significant; *P<0.05, **P<0.01, ***P<0.001. NES: Normalized enrichment score; mRNA: Messenger RNA; NK: Natural killer.

©Journal of Central South University (Medical Science). All rights reserved.

2.4 Implication of DAMP score in immunotherapy and targeted therapy

Except for the Riaz17 cohort, melanoma patients responding to immunotherapy all exhibited significantly lower DAMP scores in the GSE35640, Gide19, VanAllen15, PUCH and Liu19 cohorts (all $P<0.05$, Figure 5A). Further, when melanoma patients were divided into 2 subgroups by the median value of DAMP score in each dataset, patients with low DAMP score had a higher objective remission rate (ORR) to immunotherapies (Figure 5B). In addition, melanoma patients in the low-DAMP score subgroups had a significantly longer OS than those in the high-DAMP score subgroups after immunotherapy in the Gide19 cohort ($P=0.018$, Figure 5C), VanAllen15 cohort ($P=0.005$, Figure 5D), and Riaz17 cohort ($P=0.021$, Figure 5E). The analytical results of GDSC database were shown in Figure 5F to 5I. HCC patients with high DAMP score had significantly higher sensitivity scores to SB216763 (a GSK-3 inhibitor), Doramapimod (a p38α inhibitor), AZD6482 (a phosphoinositide 3-kinase inhibitor), and AZD1208 (a proviral integration Moloney virus kinase inhibitor) (all $P<0.001$).

2.5 Identification of DAMP score related hub genes in HCC

To identify hub genes which might be involved in the release of DAMPs and in the progression of ICD, weighted gene co-expression network analysis (WGCNA) was used to select gene modules highly correlated with DAMP score in both TCGA-LIHC (Figure 6A) and GSE14520 (Figure 6B) cohorts. As shown in Figure 6C, except for the grey module, the turquoise module in TCGA-LIHC ($r=0.59$, $P=3e-35$) and the brown module in GSE14520 ($r=0.47$, $P=2e-13$) were found to be most significantly positively correlated with DAMP score. Further, the "cor. geneModuleMembership" and "cor. geneTraitSignificance" in the turquoise module of TCGA-LIHC and in the brown module of GSE14520 were calculated to screen hub genes, and the thresholds were set as |cor. geneTraitSignificance| >0.5 and |cor. geneModuleMembership| >0.6 (Figure 6D and 6E). A total of 50 genes in the turquoise module of TCGA-LIHC and 7 genes in the brown module of GSE14520 met the threshold (Figure 6F). Three genes, namely centrosomal protein 55 (*CEP55*), hematological and neurological expressed 1 (*HN1*), and *TRIP13*, were identified as hub genes and exhibited strong positive correlations with DAMP score in both datasets (Figure 6G).

2.6 Exploration of the function of TRIP13 in HCC

To study the function of *TRIP13* in HCC and its impact on ICD, we first evaluated the expression of *TRIP13* in HCC. Transcriptional analyses (Figure 7A) in 3 independent datasets showed that the expression of *TRIP13* was significantly elevated in HCC when compared with normal tissues (all $P<0.001$). IHC staining of *TRIP13* in the tissue chip (Figure 7B) also revealed that *TRIP13* was dramatically upregulated in the tumor tissues ($P<0.001$). Next, we constructed HepG2 and LM3 cells with stable knockdown or overexpression of *TRIP13* using lentivirus, and Western blotting and immunofluorescence staining suggested that the interference strategies were successful (Figure 7C and 7D). EdU results suggested that overexpression of *TRIP13* in HCC cells could promote DNA synthesis and cell proliferation, while knockdown of *TRIP13* exhibited the opposite effect (Figure 7E). Figure 7F confirmed that overexpression of *TRIP13* significantly promoted *in vitro* colony formation of HCC cells, while knockdown of *TRIP13* inhibited colony formation. In addition, CCK-8 analyses (Figure 8A) also revealed that down-regulation of *TRIP13* caused lower proliferation rate of HCC cells, whereas up-regulation of *TRIP13* accelerated proliferation of HCC cells (all $P<0.001$). The results of migration ability test (Figure 8B) showed that HCC cells' migration ability was significantly enhanced after overexpression of *TRIP13*, while that was significantly weakened after knockdown of *TRIP13*.

To explore the impact of *TRIP13* on the sensitivity of HCC cells to ICD, we knocked down the expression of *TRIP13* in both HepG2 and LM3 cells and evaluated their sensitivity to 5-FU. As shown in Figure 9A, CCK-8 assay revealed that 5-FU caused more cell death in HCC cells with decreased expression of *TRIP13*. Immunofluorescence staining demonstrated that the silencing of *TRIP13* in HCC cells induced a stronger ICD response, as evidenced by enhanced *CRT* exposure and *HMGB1* release from tumor cells, which are key biomarkers of ICD (Figure 9B). Furthermore, Western blotting and immunofluorescence results (Figure 9C and

©Journal of Central South University (Medical Science). All rights reserved.

9D) indicated that knocking down *TRIP13* in HCC cells resulted in an increase in the expression of the pro-apoptotic protein Bax and a decrease in the expression of the anti-apoptotic protein Bcl-2, leading to a significantly elevated Bax/Bcl-2. This shift in the apoptotic regulatory balance is consistent with an elevated rate of cell death in HCC cells with *TRIP13* silencing after 5-FU treatment (Figure 10).

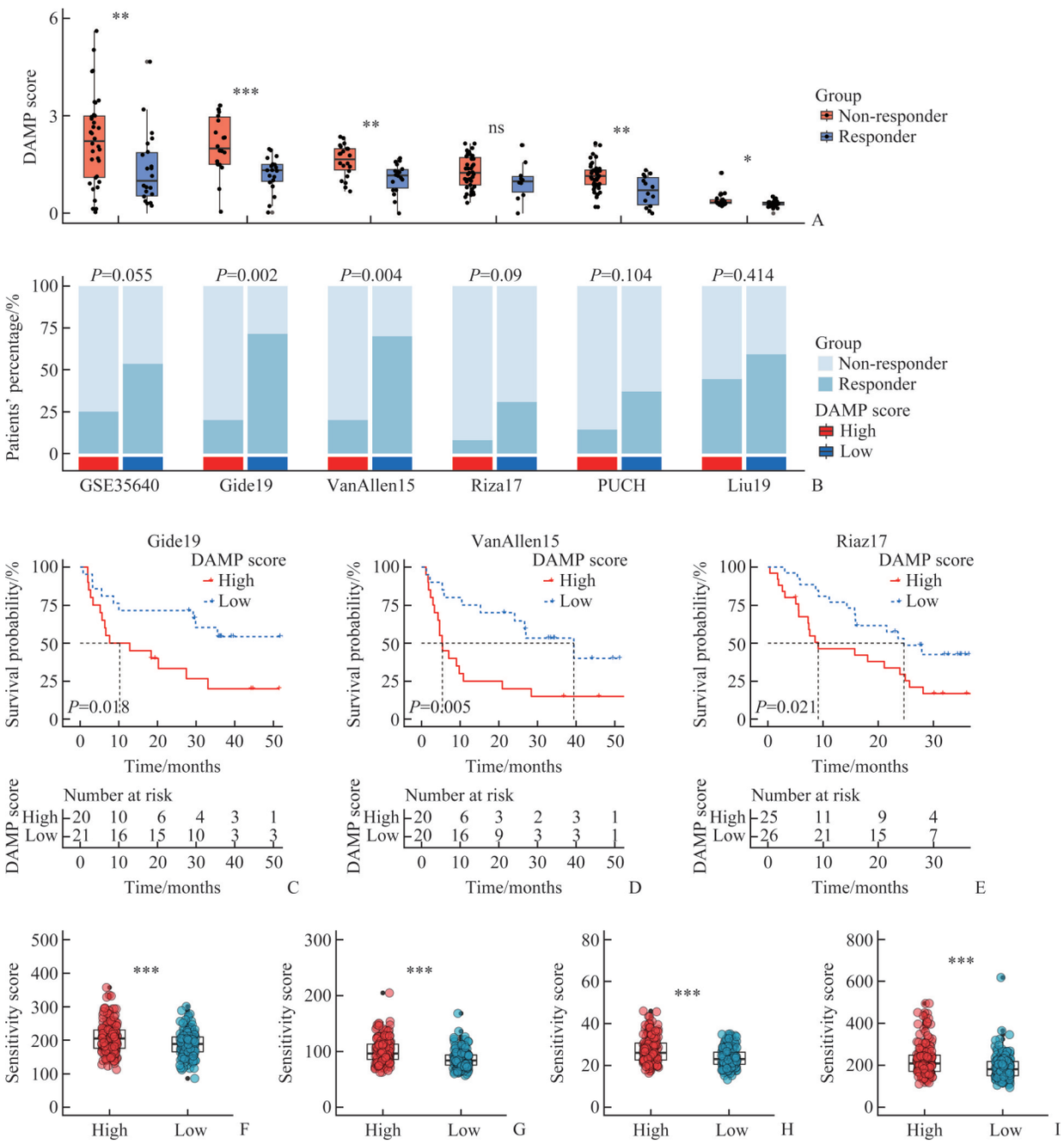


Figure 5 Implication of DAMP score in immunotherapy and targeted therapy

A: DAMP scores of melanoma patients receiving immunotherapy in GSE35640, Gide19, VanAllen15, Riaz17, PUCH, and Liu19 cohorts; B: Ratios of patients responding or not responding to immunotherapy in DAMP score stratified subgroups in GSE35640, Gide19, VanAllen15, Riaz17, PUCH, and Liu19 cohorts; C to E: Kaplan-Meier curves of OS in melanoma patients with high- and low-DAMP score from Gide19 (C), VanAllen15 (D), and Riaz17 (E) cohorts; F to I: Box plot showing the sensitivity score of SB216763 (F), Doramapimod (G), AZD6482 (H), and AZD1208 (I) in HCC patients with high- and low-DAMP score. ns: Not significant; **P*<0.05, ***P*<0.01, ****P*<0.001.

©Journal of Central South University (Medical Science). All rights reserved.

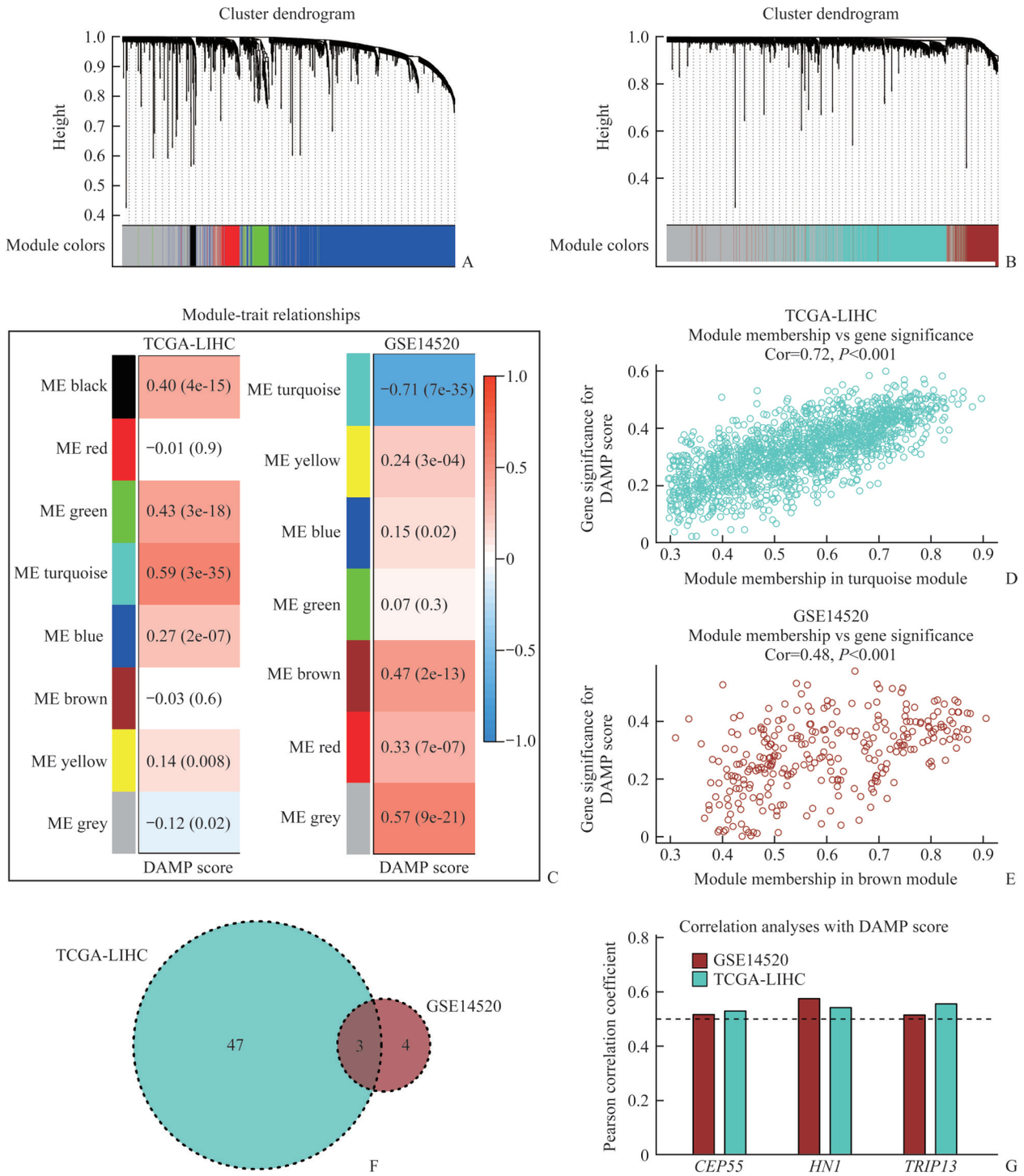


Figure 6 Identification of DAMP score related hub genes in HCC

A and B: Merging of mRNA co-expression modules in TCGA-LIHC (A) and GSE14520 (B) cohorts. C: Correlation heatmap of module genes and DAMP score in TCGA-LIHC and GSE14520 cohorts. The correlation coefficient changed from −1 to 1 as the color turned from blue to red gradually. D and E: Scatter plot of the correlation coefficient between the selected module and DAMP score in TCGA-LIHC (D) and GSE14520 (E) cohorts. F: Venn plot of hub genes of the selected module in TCGA-LIHC and GSE14520 cohorts. G: Correlation analyses between the expression of selected hub genes and DAMP score in TCGA-LIHC and GSE14520 cohorts. ME: Module eigengene; Cor: Correlation; *CEP55*: Centrosomal protein 55; *HN1*: Hematological and neurological expressed 1; *TRIP13*: Thyroid hormone receptor interactor 13.

©Journal of Central South University (Medical Science). All rights reserved.

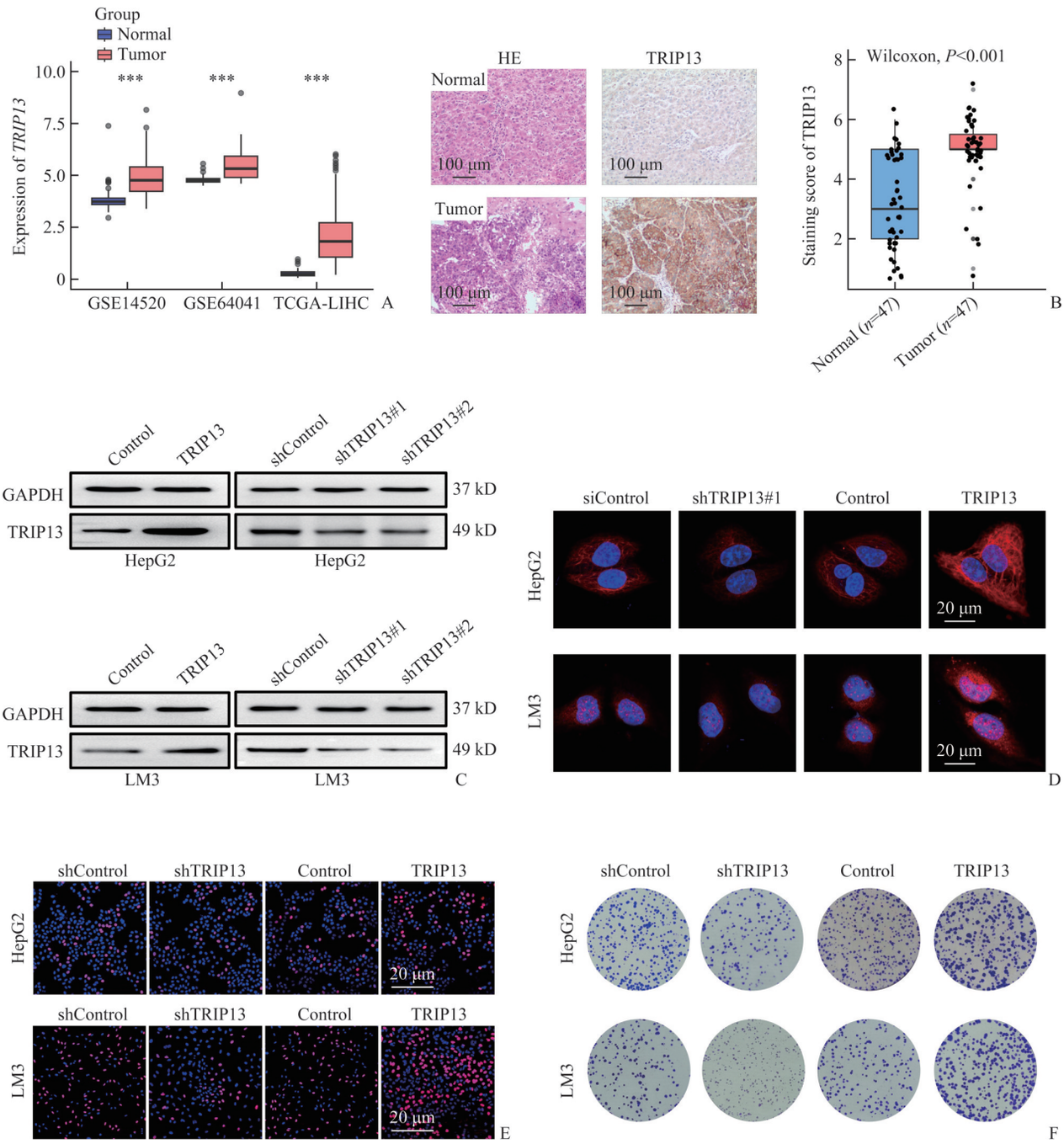
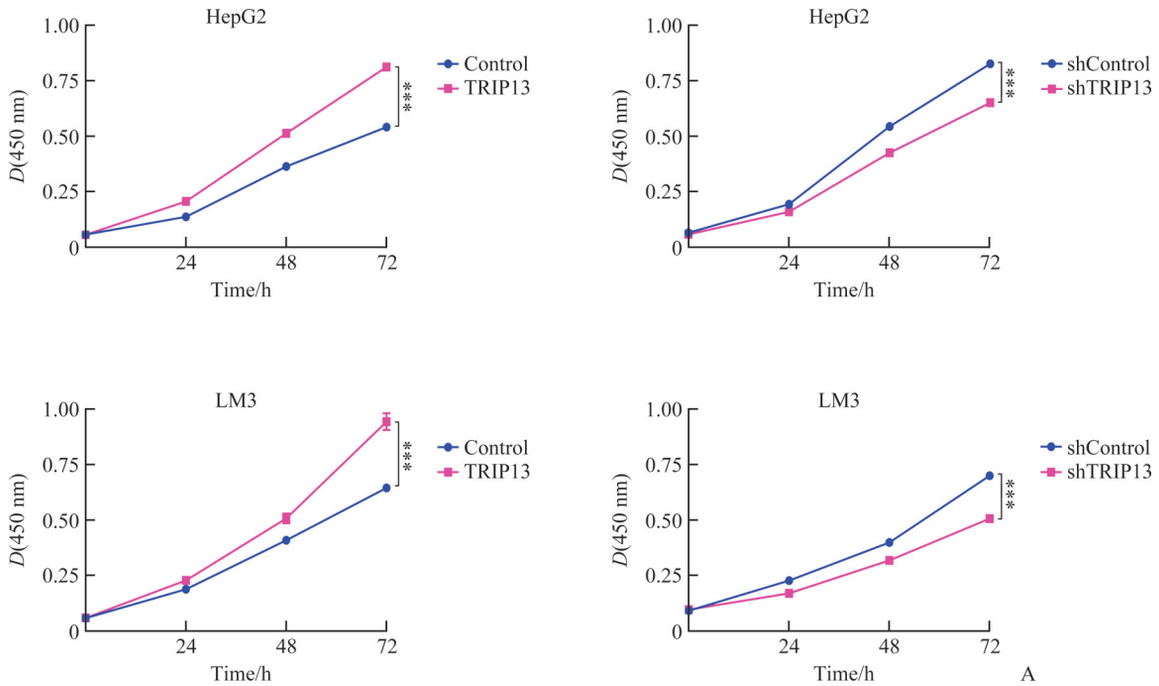


Figure 7 Oncogenic function of *TRIP13* in HCC

A: Transcriptional analyses of *TRIP13* in HCC and adjacent normal tissues from the GSE14520, GSE64041, and TCGA-LIHC cohorts; B: Representative IHC images and quantitative analysis of TRIP13 expression in a collected HCC tissue microarray; C: Western blotting analysis validating TRIP13 protein level in HCC cells after transfection with over-expression or knockdown vectors, and GAPDH served as a loading control; D: IF staining showing TRIP13 expression (green) and DAPI (blue) in HCC cells after over-expression or knockdown of *TRIP13*; E: Representative images of EdU assay assessing cell proliferation in HCC cells after modulating *TRIP13* expression (n=3 independent experiments); F: Representative images of colony formation assays in HCC cells after modulating *TRIP13* expression (n=3 independent experiments). ***P<0.001. IHC: Immunohistochemistry; HE: Hematoxylin and eosin; GAPDH: Glyceraldehyde-3-phosphate dehydrogenase; IF: Immunofluorescence; DAPI: 4’,6-Diamidino-2-phenylindole; shControl: Short hairpin RNA of control; shTRIP13: Short hairpin RNA of TRIP13.

©Journal of Central South University (Medical Science). All rights reserved.



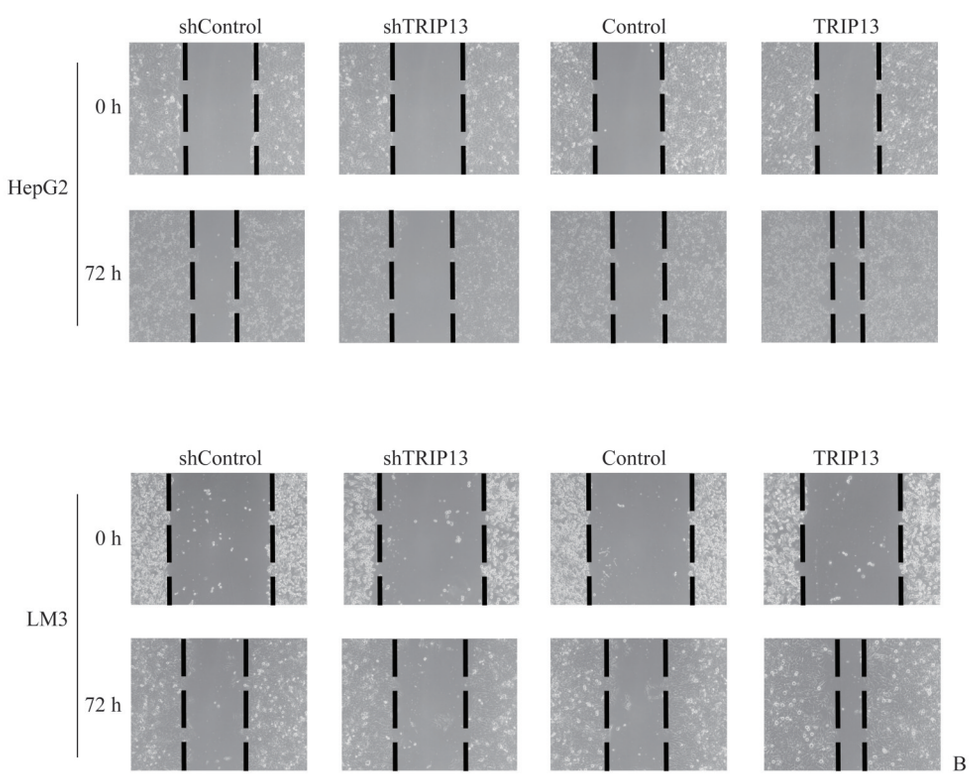


Figure 8 TRIP13 enhances HCC cell proliferation and migration

A: Cell viability measured by CCK-8 assay in HCC cells after modulating *TRIP13* expression over 72 h (n=3 independent experiments); B: Representative images and quantification of cell migration by wound healing assay in HCC cells after modulating *TRIP13* expression (n=3 independent experiments). ***P<0.001. CCK8: Cell counting kit-8; D: Optical density.

©Journal of Central South University (Medical Science). All rights reserved.

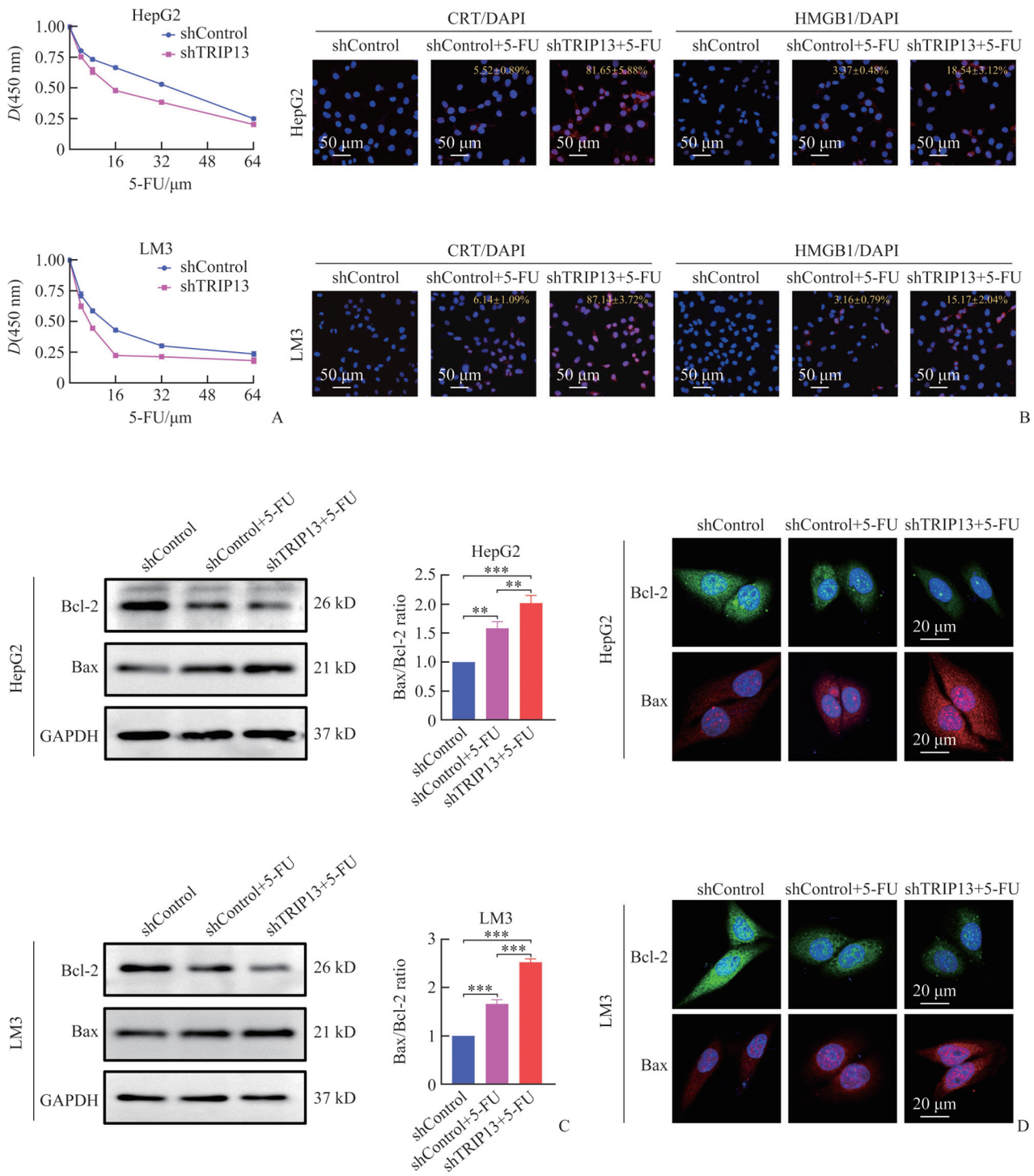


Figure 9 Impact of *TRIP13* on ICD induction and chemosensitivity

A: Cell viability measured by CCK-8 assay of HepG2 and LM3 cells in shControl and shTRIP13 after treatment with 5-FU (n=3 independent experiments). B: IF staining for ICD markers, including CRT (red, cell surface) and HMGB1 (green, nucleus/cytoplasm) in control and *TRIP13*-knockdown HCC cells after 5-FU treatment. DAPI (blue) stains nuclei. Enhanced CRT exposure and HMGB1 release are visible upon *TRIP13* knockdown. C: Western blotting analysis of the apoptosis-related proteins Bax and in control and *TRIP13*-knockdown HCC cells after 5-FU treatment. GAPDH served as a loading control. Densitometric analysis of the Bax/Bcl-2 ratio is shown on the right side (n=3 independent experiments). D: IF staining for Bax (red) and Bcl-2 (green) in control and *TRIP13*-knockdown HCC cells after 5-FU treatment. DAPI (blue) stains nuclei. **P<0.01, ***P<0.001. 5-FU: 5-Fluorouracil; ICD: Immunogenic cell death; CRT: Calreticulin; HMGB1: High mobility group box-1; Bcl-2: B-cell lymphoma 2; Bax: Bcl-2-associated X protein.

©Journal of Central South University (Medical Science). All rights reserved.

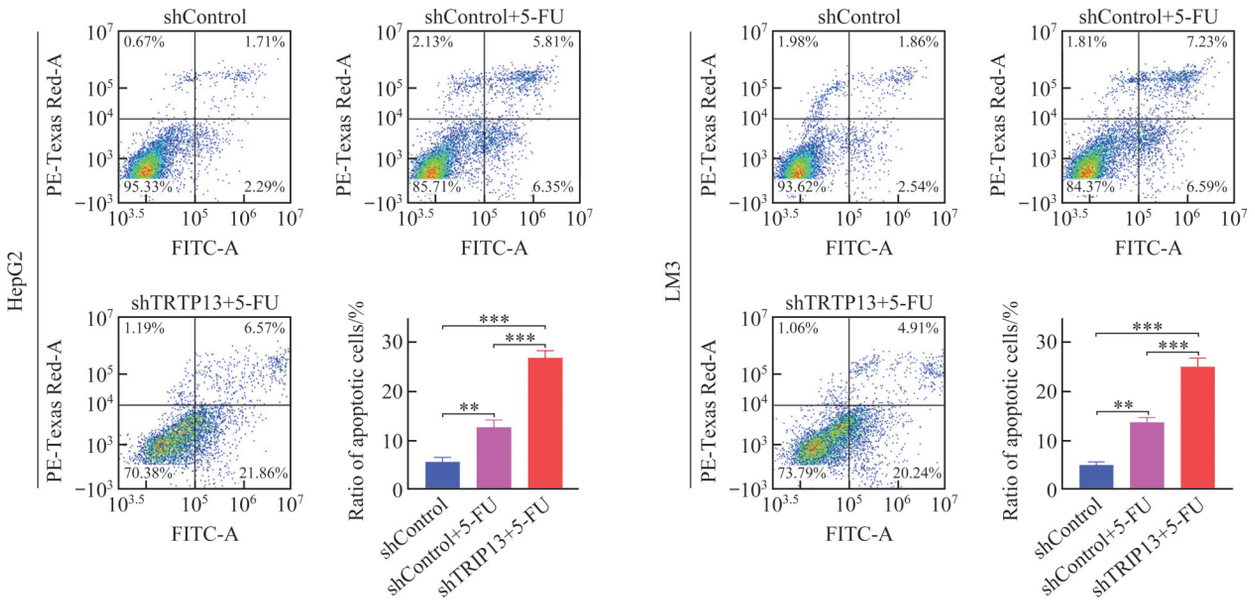


Figure 10 *TRIP13* knockdown enhances 5-FU-induced apoptosis in HCC cells

Flow cytometry analysis of apoptosis in control and *TRIP13*-knockdown HCC cells after 5-FU treatment. The bar graph shows the quantification of total apoptotic cells during early (left) and late apoptosis (right) (n=3 independent experiments). **P<0.01, ***P<0.001. PE-Texas-Red-A: Phycoerythrin-Texas-Red tandem dye-area; FITC-A: Fluorescein isothiocyanate-area.

3 Discussion

Immunotherapy brings considerable benefit to patients with several types of cancer[34-36]. However, early phase 3 clinical trials showed that ICIs alone, either pembrolizumab or nivolumab, failed to improve OS in HCC patients[37-38]. Although a recent randomized, double-blind, phase 3 trial found that HCC patients from Asia receiving pembrolizumab had significantly longer median OS than those in the placebo group[39], the difference in the time (14.6 vs 13.0 months) might be far from satisfactory from the perspective of clinicians. On the other hand, combination therapy, such as atezolizumab plus bevacizumab or lenvatinib plus pembrolizumab, extended survival time of HCC patients[40-42], suggesting HCC patients require external regimens to initiate and boost immune response.

ICD plays an important role in converting "cold" tumor into "hot" one by eliciting adaptive immunity[43]. Attempts have been made in the design of anti-cancer agents against HCC by inducing ICD. For instance, nanoparticle containing icaritin and doxorubicin efficiently improved anti-cancer effect in HCC by remodeling the immunosuppressive TME and triggering a robust immune memory response[44]. Micheliolide, a natural guaianolide sesquiterpene lactone, could induce ICD-associated DAMPs, stimulate infiltration of cytotoxic immune cells, and has a potential application in clinics by promoting long-term anti-HCC immunity[45]. However, not all tumor cells respond well to this strategy by eliciting an anti-tumor T-cell immunity through ICD-inducers[13]. DAMP is pivotal in the occurrence of ICD. In this work, we noticed that HCC patients could be classified into 2 subgroups by consensus clustering based on the expression of DAMP-related genes. HCC patients in the C1 cluster had significantly shorter survival and exhibited lower expression of most DAMP-related genes. Further, we constructed a DAMP-related risk score (DAMP score) via a set of bioinformatics analyses. HCC patients with high DAMP score were associated with worse prognosis in the training and 2 independent validating cohorts. In addition, the AUC value of DAMP score in predicting OS of HCC patients was 0.69 to 0.78, suggesting a strong capability in predicting prognosis of HCC patients. DAMP score also exhibited better performance in predicting prognosis of HCC patients than a set of clinical features including T stage, tumor stage, age,

©Journal of Central South University (Medical Science). All rights reserved.

among others. Moreover, we compared the C-index of DAMP score and that of 53 previously published mRNA signatures based on multiple biological processes, such as hypoxia[25-26], m^{6}A RNA methylation[27], pyroptosis[28], and ferroptosis[29], and found that DAMP score also had an advantage over most published mRNA risk models in predicting OS of HCC patients. Taken together, DAMP score had good potential to serve as a novel prognostic model in HCC.

Functional characterization revealed that patients stratified by the DAMP score exhibited distinct biological profiles. The high-DAMP score group was predominantly associated with enhanced cell proliferation pathways, reflecting a more aggressive tumor phenotype. In contrast, the low-DAMP score group displayed enrichment in metabolic processes and, importantly, a broad spectrum of immune-active pathways, including adaptive immune responses such as the B cell receptor signaling pathway and humoral immunity. This suggests that the DAMP score effectively distinguishes between a "proliferative-dominant" and an "immune-metabolic" phenotype within HCC.

The robust immune landscape observed in the low-DAMP score group, characterized by features like phagocytic recognition and adaptive immune activation, is highly consistent with the establishment of an immunologically active tumor micro-environment, which is a key consequence of effective ICD. ICD is able to elicit immune reaction, and in this work, DAMP score indeed exhibited a tight correlation with infiltration of immune cells, particularly CD8$^+$ T cells. While our bioinformatic analyses strongly suggest a link between a low DAMP score and an ICD-conducive phenotype, direct experimental evidence establishing the DAMP score as a biomarker for ICD induction in HCC remains to be fully elucidated and represents a valuable direction for future investigation. CD8$^+$ T cells are key players in immune system-mediated tumor cell destruction, and numerous studies[46-48] revealed that their presence in the tumor could predict immune responses to ICIs across several types of cancer. Analyses of public melanoma cohorts revealed that patients responding to ICIs tended to have lower DAMP scores, and those with high DAMP scores showed significantly shorter survival after ICIs treatment. This suggests a potential association between DAMP score and immunotherapy response. However, considering the distinct immune micro-environment of melanoma and HCC, this observation derived from melanoma data requires cautious interpretation and, more importantly, further validation in HCC-specific cohorts. For HCC patients with high DAMP score, targeted therapy, such as SB216763, AZD6482 and AZD1208, might be potentially effective anti-cancer options since these patients might benefit little from ICIs. Currently, pre-clinical studies have revealed that these drugs could inhibit cell proliferation and invasion, and cause cell death and tumor shrinkage in several types of cancer[49-54]. Undoubtedly, more experiments and clinical trials are required to confirm their anti-tumor efficacy in HCC, particularly in those with high DAMP score.

It is worth noting that mRNA signatures based on ICD or DAMP-related genes have been constructed in other types of cancer[14-17, 55-56]. For instance, Xiaoyan Li, et al[14] constructed novel ICD-related signatures in uveal melanoma (UVM) via a set of bioinformatics tools. UVM patients with high ICD score exhibited significantly shorter survival but were characterized by a substantial increase in the levels of immune cells, leading to a higher response rate to immunotherapy[14]. In another study, Ming Xu, et al[17] revealed that patients with triple-negative breast cancer could be classified into three subtypes based on expression of DAMP-related genes, and one subtype, namely the inflammatory DAMPs subtype, was predicted to have the highest response rate to immunotherapy. Taken together, our work and other studies all indicated that ICD or DAMP-related genes have the potential to identify subgroups of cancer patients who might be suitable for the ICD-inducing strategy and immunotherapy.

Finally, we identified the hub genes of DAMP score in HCC by WGCNA. *CEP55*, a pivotal component of abscission, was found to be upregulated in lung cancer, liver cancer and endometrial cancer[57-59] and involved in tumorigenesis[60]. *HN1* was overexpressed in HCC and functioned as an oncogene in the disease by

©Journal of Central South University (Medical Science). All rights reserved.

sustaining persistent activity of MYC via interaction with glycogen synthase kinase (GSK)3β[61]. Previous studies revealed that *TRIP13* plays an oncogenic role in various types of cancer, including colorectal cancer[62], B cell malignancies[63], glioblastoma[64], and lung cancer[64-65]. Recently, Marcos Rios Garcia, et al[66] reported that depletion of *TRIP13* in HCC cells induced accumulation of lipid droplets via the insulin-receptor/protein kinase B pathway, resulting in mitotic cell death and increased sensitivity to mitosis-targeting drugs such as paclitaxel. On the other hand, *TRIP13* was also identified as a key gene associated with immune cell infiltration in HCC[67-68]. In this work, transcriptional analyses across 3 independent HCC-related cohorts and IHC staining in collected HCC tissue chips showed that *TRIP13* was significantly up-regulated in HCC. Over-expression of *TRIP13* in HCC cells resulted in a more proliferative and aggressive phenotype, whereas silencing the gene in these cells led to reduced growth and migration of cells. Moreover, downregulation of *TRIP13* in HCC cells led to decreased cell death after treatment with 5-FU, an ICD-inducer in HCC[32], further suggesting that *TRIP13* regulates the sensitivity to ICD-inducers in the disease.

In conclusion, a stable and powerful DAMP-related signature was constructed and validated in HCC for prognosis and prediction of immunotherapy response. *TRIP13*, a hub gene of DAMP score, functioned as an oncogene in HCC and regulated sensitivity to 5-FU. The DAMP score-based subtype system and *TRIP13*-targeted therapy might provide novel implications for personalized anti-cancer strategies in HCC.

Contributions: HU Hao and YUAN Lehong Experimental operation, data analysis, and paper modification; SONG Zewen and TAN Juan Bioinformatics support and paper modification; NI Zixuan Literature search and paper modification; LIU Yang Research design, experimental operation, data analysis, paper writing and modification; ZHANG Xi Research design, data analysis, and paper modification. The final version of the manuscript has been approved and read by all authors.

Conflict of interest: The authors declare that they have no conflicts of interest to disclose.

References

[1] Helmberger T. Leitlinie zum hepatozellulären karzinom[J]. Radiologe, 2022, 62(3): 197-199. https://doi.org/10.1007/s00117-022-00978-9.

[2] Chidambaranathan-Reghupaty S, Fisher PB, Sarkar D. Hepatocellular carcinoma (HCC): Epidemiology, etiology and molecular classification[J]. Adv Cancer Res, 2021, 149: 1-61. https://doi.org/10.1016/bs.acr.2020.10.001.

[3] Asghar U, Meyer T. Are there opportunities for chemotherapy in the treatment of hepatocellular cancer?[J]. J Hepatol, 2012, 56(3): 686-695. https://doi.org/10.1016/j.jhep.2011.07.031.

[4] Sangro B, Sarobe P, Hervás-Stubbs S, et al. Advances in immunotherapy for hepatocellular carcinoma[J]. Nat Rev Gastroenterol Hepatol, 2021, 18(8): 525-543. https://doi.org/10.1038/s41575-021-00438-0.

[5] Shen Y, Bai X, Zhang Q, et al. Oncolytic virus VG161 in refractory hepatocellular carcinoma[J]. Nature, 2025, 641(8062): 503-511. https://doi.org/10.1038/s41586-025-08717-5.

[6] Yarchoan M, Gane EJ, Marron TU, et al. Personalized neoantigen vaccine and pembrolizumab in advanced hepatocellular carcinoma: a phase 1/2 trial[J]. Nat Med, 2024, 30(4): 1044-1053. https://doi.org/10.1038/s41591-024-02894-y.

[7] Donne R, Lujambio A. The liver cancer immune microenvironment: Therapeutic implications for hepatocellular carcinoma[J]. Hepatology, 2022, 77(5): 1773-1796. https://doi.org/10.1002/hep.32740.

[8] Ahmed A, Tait SWG. Targeting immunogenic cell death in cancer[J]. Mol Oncol, 2020, 14(12): 2994-3006. https://doi.org/10.1002/1878-0261.12851.

[9] Fucikova J, Kepp O, Kasikova L, et al. Detection of immunogenic cell death and its relevance for cancer therapy[J]. Cell Death Dis, 2020, 11(11): 1013. https://doi.org/10.1038/s41419-020-03221-2.

[10] Tzogani K, Penttilä K, Lähteenvuo J, et al. EMA review of belantamab mafodotin (blenrep) for the treatment of adult patients with relapsed/refractory multiple myeloma[J]. Oncologist, 2021, 26(1): 70-76. https://doi.org/10.1002/onco.13592.

[11] Markham A. Lurbinectedin: first approval[J]. Drugs, 2020, 80(13): 1345-1353. https://doi.org/10.1007/s40265-020-01374-0.

[12] Zhang W, Liu T, Jiang L, et al. Immunogenic cell death-related gene landscape predicts the overall survival and immune infiltration status of ovarian cancer[J]. Front Genet, 2022, 13: 1001239. https://doi.org/10.3389/fgene.2022.1001239.

[13] Yamazaki T, Hannani D, Poirier-Colame V, et al. Defective immunogenic cell death of HMGB1-deficient tumors: compensatory therapy with TLR4 agonists[J]. Cell Death

©Journal of Central South University (Medical Science). All rights reserved.

Differ, 2014, 21(1): 69-78. https://doi.org/10.1038/cdd.2013.72.

[14] Li X, Kang J, Yue J, et al. Identification and validation of immunogenic cell death-related score in uveal melanoma to improve prediction of prognosis and response to immunotherapy[J]. Aging, 2023, 15(9): 3442-3464. https://doi.org/10.18632/aging.204680.

[15] Li G, Zhang H, Zhao J, et al. Machine learning-based construction of immunogenic cell death-related score for improving prognosis and response to immunotherapy in melanoma[J]. Aging, 2023, 15(7): 2667-2688. https://doi.org/10.18632/aging.204636.

[16] Sun Z, Jiang H, Yan T, et al. Identification of immunogenic cell death-related signature for glioma to predict survival and response to immunotherapy[J]. Cancers, 2022, 14(22): 5665. https://doi.org/10.3390/cancers14225665.

[17] Xu M, Lu J, Zhong Y, et al. Immunogenic cell death-relevant damage-associated molecular patterns and sensing receptors in triple-negative breast cancer molecular subtypes and implications for immunotherapy[J]. Front Oncol, 2022, 12: 870914. https://doi.org/10.3389/fonc.2022.870914.

[18] Gan X, Tang X, Li Z. Identification of immunogenic cell-death-related subtypes and development of a prognostic signature in gastric cancer[J]. Biomolecules, 2023, 13(3): 528. https://doi.org/10.3390/biom13030528.

[19] Cui C, Xu C, Yang W, et al. Ratio of the interferon-γ signature to the immunosuppression signature predicts anti-PD-1 therapy response in melanoma[J]. NPJ Genom Med, 2021, 6(1): 7. https://doi. org/10.1038/s41525-021-00169-w.

[20] Zhang J, Zhang X, Li J, et al. Systematic analysis of the ABC transporter family in hepatocellular carcinoma reveals the importance of ABCB6 in regulating ferroptosis[J]. Life Sci, 2020, 257: 118131. https://doi.org/10.1016/j.lfs.2020.118131.

[21] Zhang Z, Zeng X, Wu Y, et al. Cuproptosis-related risk score predicts prognosis and characterizes the tumor microenvironment in hepatocellular carcinoma[J]. Front Immunol, 2022, 13: 925618. https://doi.org/10.3389/fimmu.2022.925618.

[22] Garg AD, De Ruysscher D, Agostinis P. Immunological metagene signatures derived from immunogenic cancer cell death associate with improved survival of patients with lung, breast or ovarian malignancies: a large-scale meta-analysis [J/OL]. OncoImmunology, 2016, 5(2): e1069938[2025-10-07]. https://doi.org/10.1080/2162402X.2015.1069938.

[23] Wilkerson MD, Hayes DN. ConsensusClusterPlus: a class discovery tool with confidence assessments and item tracking [J]. Bioinformatics, 2010, 26(12): 1572-1573. https://doi.org/10.1093/bioinformatics/btq170.

[24] Liu Y, Zhang X, Zhang JJ, et al. Development and validation of a combined ferroptosis and immune prognostic classifier for hepatocellular carcinoma[J]. Front Cell Dev Biol, 2020, 8: 596679. https://doi.org/10.3389/fcell.2020.596679.

[25] Hu B, Yang X, Sang X. Development and verification of the hypoxia-related and immune-associated prognosis signature for hepatocellular carcinoma[J]. J Hepatocell Carcinoma, 2020, 7: 315-330. https://doi.org/10.2147/jhc.s272109.

[26] Li Q, Jin L, Jin M. Novel hypoxia-related gene signature for risk stratification and prognosis in hepatocellular carcinoma[J]. Front Genet, 2021, 12: 613890. https://doi.org/10.3389/fgene.2021.613890.

[27] Li Z, Li F, Peng Y, et al. Identification of three m6A-related mRNAs signature and risk score for the prognostication of hepatocellular carcinoma[J]. Cancer Med, 2020, 9(5): 1877-1889. https://doi.org/10.1002/cam4.2833.

[28] Jin Y, Pu X, Ping D, et al. A pyroptosis-related gene signature predicts prognosis and immune microenvironment in hepatocellular carcinoma[J]. World J Surg Oncol, 2022, 20(1): 179. https://doi.org/10.1186/s12957-022-02617-y.

[29] Zhao C, Zhang Z, Tao J. A novel ferroptosis-related signature for prediction of prognosis, immune profiles and drug sensitivity in hepatocellular carcinoma patients[J]. Curr Oncol, 2022, 29 (10): 6992-7011. https://doi.org/10.3390/curroncol29100550.

[30] Yoshihara K, Shahmoradgoli M, Martínez E, et al. Inferring tumour purity and stromal and immune cell admixture from expression data[J]. Nat Commun, 2013, 4: 2612. https://doi.org/10.1038/ncomms3612.

[31] Zhang J, Li HY, Tao WJ, et al. GseaVis: an R package for enhanced visualization of gene set enrichment analysis in biomedicine[J]. Med Res, 2025, 1(1): 131-135. https://doi.org/10.1002/mdr2.70000.

[32] Xu D, Wang Y, Wu J, et al. MTIF2 impairs 5 fluorouracil-mediated immunogenic cell death in hepatocellular carcinoma *in vivo*: Molecular mechanisms and therapeutic significance[J]. Pharmacol Res, 2021, 163: 105265. https://doi. org/10.1016/j.phrs.2020.105265.

[33] Tan J, Liu W, Li J, et al. Over-expressed RHEB promotes the progression of pancreatic adenocarcinoma[J]. Life Sci, 2021, 277: 119462. https://doi.org/10.1016/j.lfs.2021.119462.

[34] Wolchok JD, Chiarion-Sileni V, Gonzalez R, et al. Long-term outcomes with nivolumab plus ipilimumab or nivolumab alone versus ipilimumab in patients with advanced melanoma[J]. J Clin Oncol, 2022, 40(2): 127-137. https://doi.org/10.1200/jco.21.02229.

[35] Socinski MA, Jotte RM, Cappuzzo F, et al. Atezolizumab for first-line treatment of metastatic nonsquamous NSCLC[J]. N Engl J Med, 2018, 378(24): 2288-2301. https://doi.org/10.1056/NEJMoa1716948.

[36] Ren Z, Xu J, Bai Y, et al. Sintilimab plus a bevacizumab biosimilar ($IBI_3$05) versus sorafenib in unresectable hepatocellular carcinoma (ORIENT-32): a randomised, open-label, phase 2−3 study[J]. Lancet Oncol, 2021, 22(7): 977-990. https://doi.org/10.1016/S1470-2045(21)00252-7.

[37] Yau T, Park JW, Finn RS, et al. Nivolumab versus sorafenib in advanced hepatocellular carcinoma (CheckMate 459): a

©Journal of Central South University (Medical Science). All rights reserved.

randomised, multicentre, open-label, phase 3 trial[J]. Lancet Oncol, 2022, 23(1): 77-90. https://doi.org/10.1016/S1470-2045(21)00604-5.

[38] Finn RS, Ryoo BY, Merle P, et al. Pembrolizumab as second-line therapy in patients with advanced hepatocellular carcinoma in KEYNOTE-240: a randomized, double-blind, phase III trial[J]. J Clin Oncol, 2020, 38(3): 193-202. https://doi.org/10.1200/jco.19.01307.

[39] Qin S, Chen Z, Fang W, et al. Pembrolizumab versus placebo as second-line therapy in patients from Asia with advanced hepatocellular carcinoma: a randomized, double-blind, phase III trial[J]. J Clin Oncol, 2023, 41(7): 1434-1443. https://doi.org/10.1200/JCO.22.00620.

[40] Cheng A, Qin S, Ikeda M, et al. Updated efficacy and safety data from IMbrave150: Atezolizumab plus bevacizumab vs. sorafenib for unresectable hepatocellular carcinoma[J]. J Hepatol, 2022, 76(4): 862-873. https://doi.org/10.1016/j.jhep.2021.11.030.

[41] Finn RS, Ikeda M, Zhu AX, et al. Phase ib study of lenvatinib plus pembrolizumab in patients with unresectable hepatocellular carcinoma[J]. J Clin Oncol, 2020, 38(26): 2960-2970. https://doi.org/10.1200/jco.20.00808.

[42] Yang X, Chen B, Wang Y, et al. Real-world efficacy and prognostic factors of lenvatinib plus PD-1 inhibitors in 378 unresectable hepatocellular carcinoma patients[J]. Hepatol Int, 2023, 17(3): 709-719. https://doi.org/10.1007/s12072-022-10480-y.

[43] Jin MZ, Wang XP. Immunogenic cell death-based cancer vaccines[J]. Front Immunol, 2021, 12: 697964. https://doi.org/10.3389/fimmu.2021.697964.

[44] Yu Z, Guo J, Hu M, et al. Icaritin exacerbates mitophagy and synergizes with doxorubicin to induce immunogenic cell death in hepatocellular carcinoma[J]. ACS Nano, 2020, 14(4): 4816-4828. https://doi.org/10.1021/acsnano.0c00708.

[45] Xu Z, Xu J, Sun S, et al. Mecheliolide elicits ROS-mediated ERS driven immunogenic cell death in hepatocellular carcinoma[J]. Redox Biol, 2022, 54: 102351. https://doi.org/10.1016/j.redox.2022.102351.

[46] Wong PF, Wei W, Smithy JW, et al. Multiplex quantitative analysis of tumor-infiltrating lymphocytes and immunotherapy outcome in metastatic melanoma[J]. Clin Cancer Res, 2019, 25(8): 2442-2449. https://doi.org/10.1158/1078-0432.ccr-18-2652.

[47] Edwards J, Wilmott JS, Madore J, et al. $CD103^+$ tumor-resident $CD8^+$ T cells are associated with improved survival in immunotherapy-Naïve melanoma patients and expand significantly during anti-PD-1 treatment[J]. Clin Cancer Res, 2018, 24(13): 3036-3045. https://doi.org/10.1158/1078-0432.ccr-17-2257.

[48] Tumeh PC, Harview CL, Yearley JH, et al. PD-1 blockade induces responses by inhibiting adaptive immune resistance [J]. Nature, 2014, 515(7528): 568-571. https://doi.org/10.1038/nature13954.

[49] Brasó-Maristany F, Filosto S, Catchpole S, et al. PIM1 kinase regulates cell death, tumor growth and chemotherapy response in triple-negative breast cancer[J]. Nat Med, 2016, 22(11): 1303-1313. https://doi.org/10.1038/nm.4198.

[50] Lee M, Lee KH, Min A, et al. Pan-pim kinase inhibitor AZD1208 suppresses tumor growth and synergistically interacts with Akt inhibition in gastric cancer cells[J]. Cancer Res Treat, 2019, 51(2): 451-463. https://doi.org/10.4143/crt.2017.341.

[51] Mao D, Qiao L, Lu H, et al. B-cell translocation gene 3 overexpression inhibits proliferation and invasion of colorectal cancer SW480 cells via Wnt/β-catenin signaling pathway[J]. Neoplasma, 2016, 63(5): 705-716. https://doi.org/10.4149/neo_2016_507.

[52] Zhao HF, Wu CP, Zhou XM, et al. Correction to: Synergism between the phosphatidylinositol 3-kinase p110β isoform inhibitor AZD6482 and the mixed lineage kinase 3 inhibitor URMC-099 on the blockade of glioblastoma cell motility and focal adhesion formation[J]. Cancer Cell Int, 2021, 21(1): 403. https://doi.org/10.1186/s12935-021-02028-1.

[53] Xu PF, Yang JA, Liu JH, et al. PI3Kβ inhibitor AZD6482 exerts antiproliferative activity and induces apoptosis in human glioblastoma cells[J]. Oncol Rep, 2019, 41(1):125-132. https://doi.org/10.3892/or.2018.6845.

[54] Mazor M, Kawano Y, Zhu H, et al. Inhibition of glycogen synthase kinase-3 represses androgen receptor activity and prostate cancer cell growth[J]. Oncogene, 2004, 23(47): 7882-7892. https://doi.org/10.1038/sj.onc.1208068.

[55] Cai J, Hu Y, Ye Z, et al. Immunogenic cell death-related risk signature predicts prognosis and characterizes the tumour microenvironment in lower-grade glioma[J]. Front Immunol, 2022, 13: 1011757. https://doi.org/10.3389/fimmu.2022.1011757.

[56] Wang X, Wu S, Liu F, et al. An immunogenic cell death-related classification predicts prognosis and response to immunotherapy in head and neck squamous cell carcinoma[J]. Front Immunol, 2021, 12: 781466. https://doi.org/10.3389/fimmu.2021.781466.

[57] Zhang X, Xu Q, Li E, et al. CEP55 predicts the poor prognosis and promotes tumorigenesis in endometrial cancer by regulating the Foxo1 signaling[J]. Mol Cell Biochem, 2023, 478(7): 1561-1571. https://doi.org/10.1007/s11010-022-04607-w.

[58] Liu L, Mei Q, Zhao J, et al. Suppression of CEP55 reduces cell viability and induces apoptosis in human lung cancer[J]. Oncol Rep, 2016, 36(4): 1939-1945. https://doi.org/10.3892/or.2016.5059.

[59] Yang L, He Y, Zhang Z, et al. Upregulation of CEP55 predicts dismal prognosis in patients with liver cancer[J]. BioMed Res Int, 2020, 2020: 4139320. https://doi.org/10.1155/2020/4139320.

[60] Jeffery J, Sinha D, Srihari S, et al. Beyond cytokinesis: the emerging roles of CEP55 in tumorigenesis[J]. Oncogene, 2016, 35(6): 683-690. https://doi.org/10.1038/onc.2015.128.

[61] Feng J, Liu Y, Fang T, et al. Hematological and neurological

©Journal of Central South University (Medical Science). All rights reserved.

expressed 1 (HN1) activates c-Myc signaling by inhibiting ubiquitin-mediated proteasomal degradation of c-Myc in hepatocellular carcinoma[J]. Cell Biol Int, 2023, 47(3): 560-572. https://doi.org/10.1002/cbin.11957.

[62] Agarwal S, Behring M, Kim HG, et al. TRIP13 promotes metastasis of colorectal cancer regardless of p53 and microsatellite instability status[J]. Mol Oncol, 2020, 14(12): 3007-3029. https://doi.org/10.1002/1878-0261.12821.

[63] Li C, Xia J, Franqui-Machin R, et al. TRIP13 modulates protein deubiquitination and accelerates tumor development and progression of B cell malignancies[J/OL]. J Clin Invest, 2021, 131(14): e146893[2025-10-07]. https://doi.org/10.1172/jci146893.

[64] Zhang G, Zhu Q, Fu G, et al. TRIP13 promotes the cell proliferation, migration and invasion of glioblastoma through the FBXW7/c-MYC axis[J]. Br J Cancer, 2019, 121(12): 1069-1078. https://doi.org/10.1038/s41416-019-0633-0.

[65] Cai W, Ni W, Jin Y, et al. TRIP13 promotes lung cancer cell growth and metastasis through AKT/mTORC1/c-Myc signaling [J]. Cancer Biomark, 2021, 30(2): 237-248. https://doi.org/10.3233/cbm-200039.

[66] Rios Garcia M, Meissburger B, Chan J, et al. Trip13 depletion in liver cancer induces a lipogenic response contributing to Plin2-dependent mitotic cell death[J]. Adv Sci, 2022, 9(29): 2104291. https://doi.org/10.1002/advs.202104291.

[67] Wang D, Liu J, Liu S, et al. Identification of crucial genes associated with immune cell infiltration in hepatocellular carcinoma by weighted gene co-expression network analysis [J]. Front Genet, 2020, 11: 342. https://doi. org/10.3389/fgene.2020.00342.

[68] Bin X, Luo Z, Wang J, et al. Identification of a five immune term signature for prognosis and therapy options (immunotherapy versus targeted therapy) for patients with hepatocellular carcinoma[J]. Comput Math Meth Med, 2023, 2023: 8958962. https://doi.org/10.1155/2023/8958962.

(Edited by YOU Yi)

©Journal of Central South University (Medical Science). All rights reserved.